Applied Energy 317 (2022) 119137

Contents lists available at ScienceDirect

Applied Energy

journal homepage: www.elsevier.com/locate/apenergy

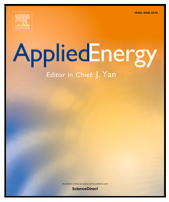

A modeling framework for predicting the effect of the operating conditions and component sizing on fuel cell degradation and performance for automotive applications

J.M. Desantes, R. Novella *, B. Pla, M. Lopez-Juarez

CMT-Motores Térmicos, Universitat Politècnica de València, Camino de vera s/n, 46022 Valencia, Spain

ARTICLE INFO

Keywords:
Hydrogen
Proton exchange membrane fuel cell vehicle
Degradation
Modeling
Sizing
Driving cycle

ABSTRACT

In this study, durability and performance prediction were integrated in the sizing process of the FC stack of a fuel cell range-extender (FCREx) vehicle together with the design of a dynamics-limited control strategy. For that purpose, a FCREx vehicle model integrating a FC stack, balance of plant, battery, H_2 tank and vehicle body (C-class SUV) validated in previous studies was used. To predict FC stack degradation rate, a novel semi-empirical multi-layered degradation modeling framework for automotive application is proposed and developed. Degradation rates are calculated based on reference degradation rates measured at reference and known conditions (1st layer) and scaled with the electrochemical phenomena (2nd layer) and the operating conditions (3rd layer) through scaling functions based on physical tendencies. Results show how increasing the FC stack power decreases H_2 consumption but increases durability, while increasing the dynamic limitations on the control strategy increases both H_2 consumption and durability. The isolated effect of sizing implied a decrease in H_2 consumption of ~3% and an increase in FC stack durability of ~53% when comparing the 40 kW and 100 kW designs. In contrast, the effect of dynamic limitations was significantly perceived in the 40 kW design which implied an increase in H_2 consumption close to 8% and an increase in durability of 294% when comparing the infinite dynamics and the highest dynamically restricted cases. Nevertheless, the effect of sizing is neglected under high dynamic limitation and limiting the current density change rate to 0.001 A/cm^2 s may prevent the control strategy from fulfilling the charge sustaining mode in aggressive driving. Based on these results, a set of recommendations were elaborated for FC stack and FCV manufacturers aiming to apply FCREx architecture to passenger car vehicles.

1. Introduction

In recent years, the use of H_2 as the main fuel in the transport sector has risen to be one of the key strategies to achieve the decarbonization of 95% of the transport sector by 2050 to limit the average global temperature increase below 2 °C with respect to 1990 levels [1,2]. The use of hydrogen fuel cell vehicles (FCV) is a clean and efficient alternative to battery electric vehicles (BEV), especially for those sectors where high range and low charging or refueling times are required and the space is limited [3]. However, its use is not limited to the automotive sector, as fuel cells can also be used for heat and power generation [4], but for that purpose proton-exchange membrane fuel cells (PEMFC) are only capable of producing up to ~100 kW. Nonetheless, there have been recent studies in which PEMFC were considered for net-zero energy communities following the vehicle-to-grid interaction [5]. In this sense, smart energy management optimization provided significant reductions of up to 1594.13 tonnes of carbon emissions [6], improvements in the renewable energy self-consumption of 18.76% [7] and in FC stack durability [8].

Recently, there have been several studies regarding the sizing of the FCV components, mainly for common FCV architectures [9]. Nonetheless, before the current scenario where the number of hydrogen refueling stations across the globe is limited [3] and the H_2 costs are significantly high the traditional FCV architecture, consisting of a small battery and a high-power FC system, may present high operation costs and low flexibility in terms of operation. In previous studies, the authors proposed the FCREx architecture for light-duty passenger cars [10], i.e., a FCV with moderate battery and variable FC system power depending on the application operating as a range-extender. This type of vehicle, also called plug-in FCV, increases the operation flexibility since part of the range can be covered using only the battery,

* Corresponding author.
E-mail address: rinoro@mot.upv.es (R. Novella).
URL: http://www.cmt.upv.es (R. Novella).

https://doi.org/10.1016/j.apenergy.2022.119137
Received 17 November 2021; Received in revised form 22 March 2022; Accepted 14 April 2022
Available online 30 April 2022

thus decreasing the dependency on H_2 refueling stations availability and costs. In previous studies, it was shown through a sizing analysis (varying the battery capacity, the FC stack maximum power and the H_2 tank capacity) how this architecture had optimum performance with high battery capacity and high FC stack power, but this design could be prohibitive in terms of cost and vehicle available space [10]. Then, the design spaces generated for that study were used to perform a life cycle assessment to understand the cradle-to-grave emissions of FCREx architecture and how they change with the components sizing. In this sense, the optimum design was found to be at moderate battery capacity and high FC stack maximum power [11]. At this point, FCREx architecture sizing was analyzed from a different perspective, but the potential to increase the durability of the FC stack of this architecture and the corresponding effect on performance when changing the FC stack maximum power or imposing dynamic limitations was not assessed, mainly due to the limited literature on FCREx vehicles and the scarcity of numerical degradation models capable of analyzing the effect of these two parameters on degradation.

Other studies have also considered the FCREx architecture for other applications such as city buses, captive fleets such as urban logistics vehicles, and trucks, but the studies that consider its use for light-duty passenger car applications are limited. In this line, Xu et al. [12] aimed at optimizing the costs and range of FCREx architecture applied to city buses considering both charge sustaining and charge depleting strategies. Through this study, the concluded that to minimize H_2 consumption the priorities are (in order): reducing balance of plant and auxiliary power, braking energy recovery, increase FC stack efficiency and decreasing battery losses. For other applications, Wu et al. [13] performed a sizing study for urban logistics FCREx by applying convex programming methodology that concluded with an optimum design consisting of a battery with an energy capacity of 29 kWh and a FC stack maximum power dependent on the H_2 cost. They then continued their research for alternative applications such as trucks by applying FCREx architecture [14], showing that convex programming methods could provide minimal H_2 consumption in 8*CHTC-HT and 7*C-WTVC Chinese truck driving cycles.

Although FCVs are an interesting option to decrease the overall greenhouse emissions in the transport sector, they have relatively low durability, compared to current internal combustion engine vehicles [15]. Entities such as the Department of Energy (DoE) of the US have set the durability 2020 targets as 40000 h for stationary applications and 5000 h under realistic driving conditions [16]. As a consequence, the modeling of such systems has been in the spotlight of the scientific community during the last years [17,18].

FC degradation must be predicted since it leads to the decrease of the FC maximum power production capability through the increase in activation, ohmic, and concentration losses, among others. Being able to capture these phenomena is especially important during dynamic operation, where the degradation mechanisms are enhanced due to load cycling. In a vehicle environment, the energy management strategy (EMS) that is in charge of properly managing the energy flows and the power split when an FC and a battery are powering simultaneously the vehicle needs to be aware of the degradation rate and degraded state of the FC to provide the optimum energy consumption. As such, developing degradation models that enable online prediction degradation is critical since it affects both the energy conversion processes, as the electrochemical losses increase, and the energy management, since the solution proposed through management optimization algorithms strongly depends on the degradation state of the powertrain components [19].

The membrane electrode assembly (MEA) is the part of the FC where all the electrochemical processes take place. It is composed of the gas diffusion layer (GDL), the cathode catalyst layer (CCL), the anode catalyst layer (ACL), and the membrane. Among these MEA subcomponents, the catalyst layers are responsible for enabling the fast H_2 decomposition into protons (H^+) and the water formation through the following reaction:

$$2H^+ + \frac{1}{2}O_2 \rightarrow H_2O$$

The energy losses that take place at the catalyst layers are those called activation losses. They are produced due to the extra energy (overpotential) that needs to be applied over the reaction surface to achieve the desired reaction rate. Part of the lost energy in the catalyst does not simply dissipate as heat but also contributes to the catalyst degradation mechanism, hence the loss of electrochemical surface area (ECSA) [20]. Among these mechanisms, it is possible to identify Pt dissolution, carbon corrosion, Ostwald ripening, Pt agglomeration, and Pt particle detachment as the main degradation mechanism [21]. All of these mechanisms are exacerbated at high temperatures [22,23].

The membrane is the component that allows the H^+ transport from anode to cathode and is responsible for the ohmic losses of the FC, mainly produced by the ionic conductivity of the membrane, which is significantly affected by the membrane water content [24]. Membrane degradation may be due to chemical or mechanical reasons such as membrane decomposition or cracking due to water content cycling [25]. These two mechanism works synergistically, so they are usually related. In order to quantify membrane chemical and overall membrane degradation, the fluoride release rate is often measured [26].

The GDL is a porous layer in charge of distributing uniformly the reactants to the catalyst layers, providing mechanical support and allowing the electrons conduction to the bipolar plates, heat dissipation, and water removal. The major losses that the GDL contributes to are the concentration losses at high current density. However, the GDL layer degradation has a minor effect on overall performance, hence catalyst layer and membrane degradation are usually the most important phenomena contributing to FC rated power decay [27].

Recently, there have been significant efforts in the literature to identify and model all the phenomena producing the degradation of the MEA in FC. Two different approaches to FC degradation modeling are usually followed: semi-empirical and analytical/physical. The first approach usually obtains data from a certain set of experimental data at reference conditions and applies them directly through the use of coefficients that mostly imply constant degradation rates that are independent of the FC stack operating conditions and electrochemical behavior. Although it is commonly done, this type of model is not suitable to predict degradation on driving cycle conditions, where the operating conditions deviate significantly from the reference conditions at the experimental tests. The second approach is analytical/physical, based on transport equations and source terms modeling effects such as the Pt loss or the change in the membrane ohmic resistance with degradation. These models are usually validated under a limited range of operating conditions and require very specific information about the FC to model degradation such as the membrane H_2 content time evolution, which is not predicted by most FC models and is currently impossible to measure during FC stack operation.

Empirical and semi-empirical FC degradation models are mostly based on the studies performed by Pei et al. [28] and Lu et al. [29]. In these studies they performed degradation tests with an FC stack, developed a degradation model that consisted of constant degradation rates, and validated it with data from a city bus operating with an FC on a daily basis. However, most of the studies that use these coefficients do not know their source nor the operating conditions of current density, temperature, and relative humidity at which they were obtained. As a consequence, they use them directly at any operating condition. These studies mostly use this degradation model to implement different EMS optimization strategies considering the degradation such as Pontryagin's Minimum Principle [30], modular EMS considering fuzzy-logic and Rainbow-based SOC prediction [31] or min–max game based EMS [32], among others. In some of these studies, the initial model was modified to with multiplying correction coefficients and

natural degradation rates, whose origin is often unknown [33]. Other alternative approaches for semi-empirical FC degradation modeling are also found in the literature but are limited and often do not include the effect of the FC operating conditions of the FC (T and RH) on degradation [34]. An example is as that developed by Ou et al. [35], whose degradation is modeled through a time-dependent exponential function affecting the exchange current density (activation losses) or the study performed by Ma et al. [36], in which they used a recurrent neural network with grid long-short term memory to predict the current modification due to degradation through the fitting of an activation function and the hyperbolic tangent of the cell state.

Apart from the models already mentioned, there are other models that try to integrate the FC operating conditions in the semi-empirical adjustment of the degradation rates. These studies often obtain experimental data from other sources or self-produced and use algorithms to match the coefficients of the functions used to scale the degradation rates. It is the case of the study performed by Chen et al. [37], which developed a FC degradation model by fitting the experimental data to semi-empirical functions relating the FC degradation to the FC current, relative humidity, temperature, and pressure though extreme machine learning, genetic algorithms and wavelet analysis. Among these methods, the one combining wavelet analysis for multiscale decomposition with genetic algorithms with extreme machine learning to build the model of each sub-waveform with mean absolute percent errors below 0.05% in its final form. Nevertheless, the predicted tendencies, although they were accurate for the validated FC, lacked of a direct relation with the physical tendencies on how the catalyst and the membrane degrades, so the linear functions may need to be recalibrated for each FC stack. Bressel et al. [38] performed a similar study by using of an extended Kalman filter to fit a linear function α(t) that was used to modify the reference ohmic resistance and limiting current density through direct multiplication of these parameters. The model was initially calibrated with the steady-state experimental data (constant load) so it was not applicable to dynamic FC operation. Nevertheless, the authors improved the model to integrate the effect of dynamic load demand on FC degradation [39].

The other approach to FC degradation modeling can be called the physical approach, since it intends to capture the detailed physical phenomena behind degradation, and model them through analytical equations. The studies following this approach are mostly focused on the catalyst degradation [40,41], or membrane degradation [42,43] only, are validated for a very specific set of operating conditions of current density, dynamic/steady behavior, temperature, relative humidity, ... and may imply high computational cost because some of them are applied by solving additional transport equations.

In this study, a degradation model is developed by combining both of the approaches explained. The idea behind this degradation model is to obtain empirical data at reference conditions or from testing protocols (semi-empirical) and to scale the measured reference degradation rates using physical tendencies through normalized functions (semi-physical). A similar approach to this model can be found in the study performed by Chen et al. [37], where the degradation of PEMFC was predicted by considering the combined effect of current density, temperature, relative humidity, and H_2 pressure. Nonetheless, the degradation scaling functions in that study were linear trends whose coefficients were calibrated using extreme machine learning and genetic algorithms. Therefore, despite the great fidelity of the model to the calibrated conditions and FCV technology, it may induce some error if it is applied to other FCV since the scaling functions were not extracted from physical trends but from a fitting.

1.1. Knowledge gaps

Considering the previous studies, some conclusions can be extracted to provide an idea of the knowledge gaps in the literature:

1. There are no studies in the literature analyzing the potential of FCREx architecture to increase FC durability, given the possibility to limit the FC stack dynamics of these vehicles due to the battery capacity. For FCREx vehicles, the dynamics may be limited through a decrease in the number of load-change cycles and the load-change intensity (rate of change of current density). Some studies [8,28] integrate only the decrease in the number of cycles but are unaware of the effect of changing the dynamics of the load-change cycles.
2. The effect of FC stack component sizing on degradation has not been assessed yet.
3. Empirical and semi-empirical degradation models do not apply correctly the degradation coefficients since they do not scale them with the electrochemical and operating conditions. Also, these models usually apply the voltage decrease uniformly across the polarization curve, which may induce some error.
4. There are no FC degradation models in the literature that are designed to capture the degradation rates in standardized testing conditions and scale them to actual driving operation with the FC operating conditions and electrochemical behavior that are transversely applicable to most of the PEMFC technologies.
5. The models that consider the operating conditions in the degradation rate prediction is often adjusted to a specific FC, and ignore the physical trends behind degradation since they are usually fitted through machine learning algorithms.
6. Most of the degradation models cannot apply the degradation rates obtained in the testing protocols since they do not include the effect over the degradation of changing the operating conditions and electrochemical behavior of the FC stack from those in the testing protocols.
7. The surveyed models are only applicable to PEMFC models and do not seem to be useful for the diagnosis of the degradation state of an experimental PEMFC after testing.
8. Some of the degradation models do not differentiate between the degradation sources from the operating conditions.

From the previous considerations, it is evident how the development of a PEMFC model closing these gaps is of great interest in order to support the further development of this technology.

2. Contribution and objectives

The main contribution of this paper consists of developing a flexible semi-empirical semi-physical degradation model than can be widely applied through the use of scaling functions based on physical trends and degradation rates measured at known reference conditions. The specific contributions of this paper are:

- Analyze the effect on durability and performance of modifying the FC stack sizing and applying dynamic restrictions on the FC behavior. Understand whether there is a cross-effect between these two parameters and elaborate recommendations for FC stack and FCV manufacturers to aid in the development of FCREx technology (knowledge gaps 1 and 2).
- Provide a methodology to scale up or down the degradation rates measured at specific conditions (knowledge gaps 3, 4, and 5) integrating an empirically-based strategy to spread the degradation effect on voltage along the polarization curve (knowledge gap 3).
- Develop a degradation model validated in real driving cycle conditions for its application in multiple sectors (knowledge gap 6) that differentiates between degradation sources during operation such as low-power, high-power, medium-power (natural), start–stop and load-changing conditions (knowledge gap 5), and applicable for both PEMFC models degradation modeling and experimental PEMFC degradation diagnosis (knowledge gap 8). This degradation model should allow the analysis of the sensitivity of FC durability to FCV components sizing and dynamic limitations (knowledge gaps 1 and 2)

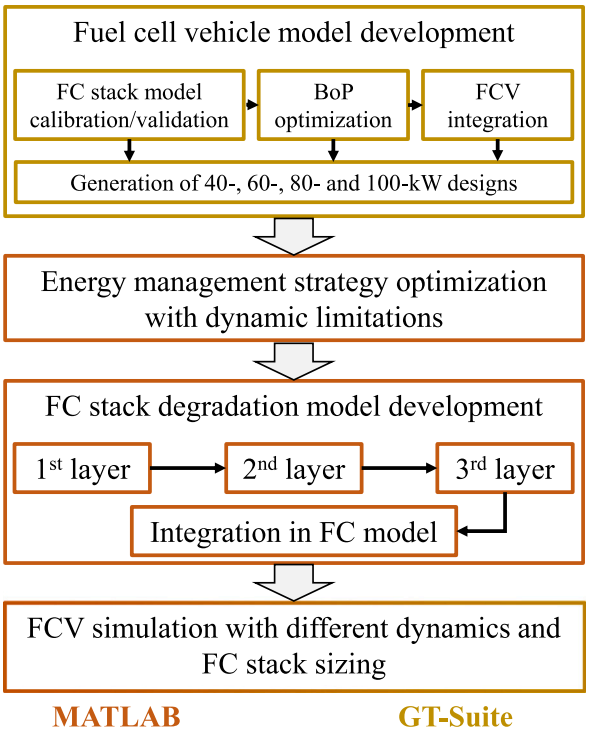

Fig. 1. Methodology outline. Activities in dark yellow were performed with GT-Suite v2020 while activities in dark orange were accomplished with MATLAB R2020a.

- Develop a degradation prediction strategy that is scalable with the PEMFC technological level and that can apply the degradation rates obtained from testing protocols through the modification of scaling functions and reference degradation rates (knowledge gap 9).

3. Methodology

In order to perform the simulations required to analyze the effect of FC stack sizing and dynamic limitations on performance and durability of FCREx vehicles, a validated FC model was used and integrated into a scalable balance of plant to conform an FC system. The management of the balance of plant components was optimized in previous studies to maximize FC system efficiency. The resulting model was integrated into an FCV architecture. In parallel, energy management optimizer algorithms and semi-empirical semi-physical degradation models were developed and integrated to perform the WLTC 3b driving cycle simulations in fair conditions. This section intends to cover all the important aspects of the modeling procedure but is focused extensively on the degradation model development as it is the main novelty in the methodology of this study. The FC stack model, the management of the balance of plant architecture, and the design of the FCV architecture were performed in previous studies and explained extensively [10,11].

For the FCV modeling, GT-Suite v2020 software was used. This numerical tool is extensively used in the automotive industry and for research purposes as it is a 0D-1D thermal fluid-dynamics modeling platform that solves the continuity, momentum, energy, and species equations numerically and applies well-known and widely accepted physically-based correlations. To complement this modeling tool, the degradation model and the energy management strategy optimizer were developed in MATLAB R2020a software and connected to GT-Suite to solve the driving cycle simulations. Fig. 1 shows schematically the structure of the methodology used to fulfill the objectives of this study

3.1. Fuel cell vehicle model

3.1.1. Vehicle architecture

Following the FCREx architecture, the vehicle model is composed of a vehicle body (C-class SUV), a scalable FC system model, an NMC111 battery pack with a capacity of 30 kWh, a 120 kW electric motor, and a H_2 tank with a capacity of 5 kg of fuel. The vehicle electronic configuration was indirect, meaning that both the FC system and the battery pack have a DC–DC converter (95% of electrical conversion efficiency) to provide power to the electric motor. This configuration is used in modern FCVs since it protects the FC from the electric oscillations coming from the DC bus and allows the FC system downsizing thanks to the voltage boost [44].

For the sizing of the FC system model, the vehicle mass was varied by considering a specific power of the FC system as a scaling factor based on commercial FC system data [45,46]. The battery was modeled as a set of 100 cylindrical cells to provide enough power to the e-motor when required grouped in 25 parallel sets to provide enough energy capacity. Each cell had a nominal voltage of 3.6 V and a capacity of 3.35 Ah.

3.1.2. Fuel cell system model

The FC system model is composed by a FC stack and all the auxiliary components required for the stack to operate in driving cycle conditions, i.e., the balance of plant (BoP). The FC stack polarization curve, describing the relation between the voltage and the current density per cell, was modeled with the following set of equations:

$$V_{FC} = V_{OC} - V_{act} - V_{ohm} - V_{conc} \tag{1}$$

$$V_{act} = \begin{cases} \frac{R_{gas}T}{2F}\left(\frac{i}{i_0}\right) \\ \frac{R_{gas}T}{2\alpha F} ln\left(\frac{i}{i_0}\right) \end{cases} \tag{2}$$

$$V_{ohm} = R\ I \tag{3}$$

$$V_{mt} = -C\ ln\left(1 - \frac{i}{i_l}\right) \tag{4}$$

where V_{OC} is the open voltage circuit and V_{act}, V_{ohm} and V_{mt} are the activation, ohmic and mass transport losses. Exchange current density (i_0) dependency with temperature, oxygen partial pressure, electrochemical reaction activation energy, electrode roughness, and reference exchange current density was modeled as in [47]. Ohmic resistance (R) was modeled by considering the change in the membrane ionic resistance with the membrane water content, based on a reference ohmic resistance, as in [24]. The reference exchange current density, reference ohmic resistance, charge transfer coefficient (α), mass transport loss coefficient (C), limiting current density (i_l), and voltage open circuit losses values were calibrated to validate the model at different conditions of pressure and temperature following the experimental data in [48,49]. GT-Suite genetic algorithms toolbox was used to calibrate the model and keep the overall error between the experimental and the numerical results below 2% (Fig. 2). Unlike other studies in the literature, the FC model was validated by matching the numerical to the experimental polarization curves at different conditions of pressure and temperature simultaneously since in driving cycle conditions the FC stack is expected to be subjected to different operating conditions depending on the environment and on the BoP components operation.

The FC model was then integrated into a balance of plant model (Fig. 3), designed and optimized in previous studies [10]. The BoP consists of a set of components for the anode, cathode, and cooling circuits. The anode circuit is composed of a H_2 tank connected to the stack through a valve to regulate the anode pressure and an active H_2 recirculation loop that drives back the fuel excess to the stack with a H_2 pump that is also used to control anode stoichiometry. The cathode circuit comprises an electric centrifugal compressor, followed by a heat exchanger to cool down the air and a humidifier to increase the air

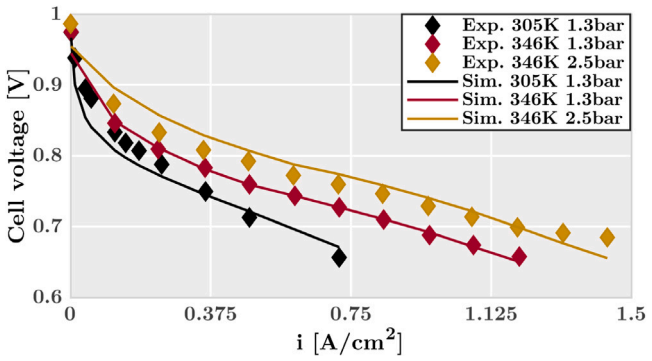

Fig. 2. FC model validation results at different temperatures and pressures. Experimental data retrieved from [48,49].

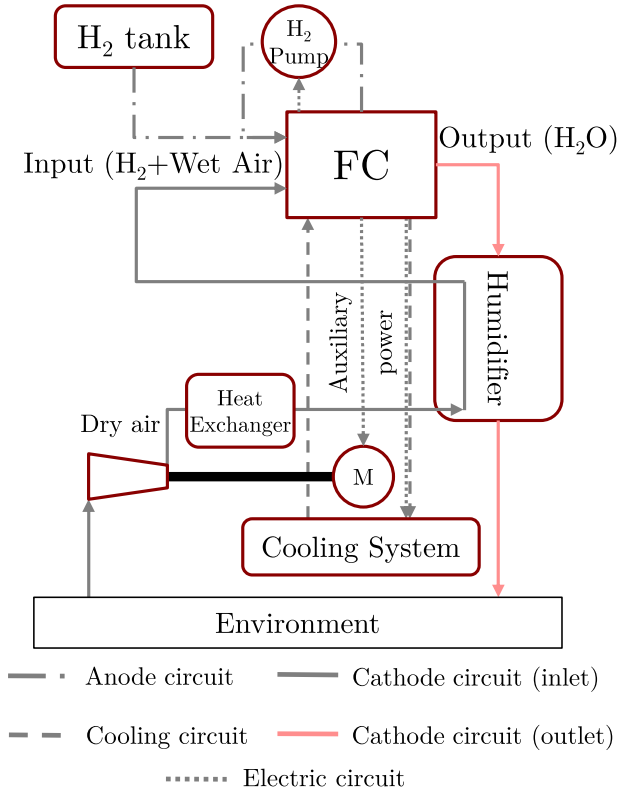

Fig. 3. FC system outline composed by the FC stack and the BoP components developed initially and optimized at [10].

relative humidity at the FC stack cathode inlet to decrease ohmic losses. The gases at the cathode outlet, mostly composed of water vapor and low-oxygen-content air, are used in the humidifier to increase the water content of the air at the cathode inlet. The air mass flow is regulated by controlling the power provided to the electric motor while the cathode pressure is controlled by modifying the throat area of a valve at the outlet of the cathode circuit. The consumption of all the components is considered in the calculations and their control is performed with PID controllers.

3.2. Energy management strategy

FCV and hybrid vehicles require the optimization of the communication between the different systems generating power in the powertrain to maximize performance. In other words, the power-split sequence or the energy management strategy needs to be optimized to make full use of the different power sources powering the vehicle [50]. In the case of FCVs, the electric power is produced both by the battery and the FC system but can only be recovered with the battery. For known driving cycle conditions, optimal control (OC) is a suitable tool to benchmark different designs and constraints over the vehicle operation, since it naturally provides the optimal energy split for every powertrain considered. In this line, OC ensures that all the powertrain architectures are compared in the best possible scenario [51].

For this study, the target function to be minimized is the H_2 consumption, under the constraint of a charge sustaining mode, i.e., battery state-of-charge (SOC) must have the same value at the beginning and at the end of the driving cycle. Therefore, the OC problem consists of finding the control strategy $u(t)$ that minimizes the cost:

$$J = \int_{t_0}^{t_f} P_f\left(u\left(t\right), t\right) \mathrm{d}t \tag{5}$$

while fulfilling the constraint:

$$\int_{t_0}^{t_f} P_b\left(u\left(t\right), E_b\left(t\right), t\right) \mathrm{d}t = 0 \tag{6}$$

where J is the cumulative H_2 consumption between times t_0 and t_f, P_f is the H_2 power spent as a function of the control variable $u(t)$, which is current density and P_b is the battery power consumption as a function of the battery energy content E_b.

To solve the OC problem Pontryagin's Minimum Principle (PMP) was considered. It consists of solving the global optimization problem as a set of local optimization problems. The PMP states that if u^* and E_b^* are the optimal trajectories of the control and battery energy over the driving cycle, then:

$$H\left(u^*, E_b^*, \lambda^*, t\right) \leq H\left(u, E_b^*, \lambda^*, t\right) \forall u \in U, t \in [t_0, t_f] \tag{7}$$

where H is the Hamiltonian function, defined as:

$$H = P_f - \lambda \dot{E}_b = P_f\left(u\left(t\right), t\right) + \lambda\left(t\right) P_b\left(u\left(t\right), E_b\left(t\right), t\right) \tag{8}$$

Note that the dimensionless co-state λ can be set as constant since the battery parameters (open circuit voltage and internal ohmic resistance) present a small dependency with the battery energy content E_b or SOC [52]. Therefore, the optimization problem consists of iterating the value of λ for the driving cycle until the charge sustaining condition (Eq. (6)) is fulfilled while minimizing the cost function H each time step.

Dynamic limitations on |di/dt| were imposed through the Hamiltonian function by adding the term L that turned infinite for all the values of the control variable u that implied higher dynamics than desired:

$$H = P_f - \lambda \dot{E}_b + L \tag{9}$$

$$L = \begin{cases} 0 & |\mathrm{di/dt}|(t + dt) \leq |\mathrm{di/dt}|_{max} \\ inf & |\mathrm{di/dt}|(t + dt) > |\mathrm{di/dt}|_{max} \end{cases} \tag{10}$$

This energy management strategy is used in this study to find the optimum control sequence that minimizes H_2 in WLTC 3b cycles provided that some constraints are imposed in the dynamics of the FC stack operation to maximize its durability. This is applied over an FCREx architecture integrated into an SUV-type vehicle based on Hyundai Nexo FCV, as detailed in [11]. For that purpose, the simulation platform developed in previous studies and explained in Section 3.1 was used to simulate the vehicle with WLTC 3b driving cycle velocity profile with different FC stack dynamic constraints and FC stack sizing. The implications of applying different stack sizing and dynamics can be perceived in Fig. 14 and are discussed in detail in terms of consumption and durability in Section 4.

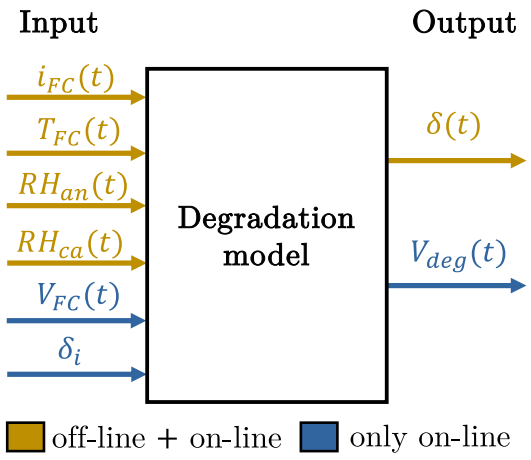

Fig. 4. Inputs–outputs diagram.

3.3. Degradation model

The purpose of this degradation model is to identify, quantify and implement on FC models the degradation effect on the performance of any PEMFC operating in dynamic conditions. This model can be used both in experimental and simulation activities. In the case of experimental activities, the model can analyze basic data from the FC stack and provide a diagnosis about how much the FC stack has been degraded during its operation, i.e., the model would be implemented off-line. In the case of simulation activities, the degradation model can be connected in parallel to the FC stack model and simultaneously modify the voltage output of the system by analyzing in real-time the operating conditions of the FC model, i.e., it would be an on-line implementation. For the latter application, the control strategy of the FC stack should be aware of how the degradation model affects the voltage so that the FC model can correct the current density for a given power demand or consider the voltage and the current as separate outputs to produce a certain power. In this case, the output voltage of the FC stack in the FC system modeling platform should be decreased by applying the degraded voltage ratio or FC stack voltage loss ($\delta = 1 - V_{deg}/V_{FC}$), which is an output of the degradation model, and the power calculated from the degraded voltage and the current produced by the stack, thus implying a decrease in the power-production capabilities of the stack. In this sense, the FC system and degradation model should work in parallel in such a way that the degraded voltage ratio is updated each time step based on the operation of the FC.

As commented before at the introduction section, the physical PEMFC degradation models focus on difficult or impossible-to-measure parameters such as the real-time concentration of H_2 in the membrane while the empirical or semi-empirical degradation models only rely on the current density of the fuel cell stack and apply constant degradation rates without considering the physical conditions nor electrochemical behavior of the FC stack. This degradation model was developed as a combination of both approaches: semi-empirical and semi-physical. As such, the output of the degradation model is the FC stack voltage loss (δ) and/or the degraded FC voltage (V_{deg})) while the inputs are the FC stack current density (i), temperature (T_{FC}) cathode and anode relative humidity (RH_{an}&RH_{ca}) for the off-line implementation and the same inputs plus the FC stack voltage (V_{FC}) and the initial degradation state of the stack (δ_i) for the on-line implementation (Fig. 4).

The main idea behind this degradation model is to scale-up or scale-down reference degradation rates obtained from a known experimental procedure, where the operating conditions such as T_{FC} and the corresponding RH are controlled while the test characteristics (i and its evolution with time) are known. This model architecture would allow to directly apply the results from the standardized FC recent development of FC stack technology and the associated regulation, this type of approach is necessary since these tests are performed at very specific conditions that are significantly different from those occurring when an FC system is used in a real application [53,54]. Therefore, in order to include these features, this model architecture consists of three different layers represented by a set of linearly independent equations, each one of them representing the effects of a particular condition (1st layer) or physical/electrochemical phenomena (2nd and 3rd layers) on FC voltage degradation. The overall voltage degradation was described by the independent effects of low-power/idle (δ_{lp}), load-change (δ_{lc}), high-power (δ_{hp}), natural degradation (δ_{nt}), and start–stop (δ_{ss}) conditions on degradation.

$$\delta = \int_0^t \left[\left.\frac{d\delta}{dt}\right|_{lp} + \left.\frac{d\delta}{dt}\right|_{lc} + \left.\frac{d\delta}{dt}\right|_{hp} + \left.\frac{d\delta}{dt}\right|_{nt} \right] dt + \frac{d\delta_{ss}}{dn_{ss}} n_{ss} \tag{11}$$

$$\left.\frac{d\delta}{dt}\right|_{lp} = \left.\frac{d\delta}{dt}\right|_{lp,ref} \cdot \xi_{lp}(i) \cdot \tau(T_{FC}) \cdot \eta(\overline{RH}) \tag{12}$$

$$\left.\frac{d\delta}{dt}\right|_{lc} = \left.\frac{d\delta}{dn_{lc}}\right|_{ref} \cdot \xi_{lc}\left(\frac{di}{dt}\right) \cdot \tau(T_{FC}) \cdot \eta(\overline{RH}) \tag{13}$$

$$\left.\frac{d\delta}{dt}\right|_{hp} = \left.\frac{d\delta}{dt}\right|_{hp,ref} \cdot \xi_{hp}(i) \cdot \tau(T_{FC}) \cdot \eta(\overline{RH}) \tag{14}$$

$$\left.\frac{d\delta}{dt}\right|_{nt} = \frac{\left.\frac{d\delta}{dt}\right|_{hp,ref} \xi_{hp}(i_{hp}) - \left.\frac{d\delta}{dt}\right|_{lp,ref} \xi_{lp}(i_{lp})}{i_{hp} - i_{lp}} (i - i_{lp}) + \left.\frac{d\delta}{dt}\right|_{lp,ref} \xi_{lp}(i_{lp}) \tag{15}$$

$$\frac{d\delta_{ss}}{dn_{ss}} = \left.\frac{d\delta}{dn_{ss}}\right|_{ref} \tag{16}$$

where i, $\frac{di}{dt}$, T_{FC} and $\overline{RH}$ are dependent on time since they are obtained from the operating conditions and the BoP management. $\overline{RH}$ is the average relative humidity between the cathode and the anode, n_{ss} is the number of star-stops in a given driving cycle, i_{lp} is the maximum current density for which low-power degradation is not negligible, and i_{hp} is the minimum current density for which high-power degradation is not negligible. Note that ξ, τ, and η are scaling functions whose value is 1 when the FC stack is operating under the same reference conditions of the test where the reference degradation rates were obtained. In this case, the natural degradation rate is not affected by the operating conditions of temperature and relative humidity since, by definition, it is present no matter how the FC is operated. Nonetheless, it is modeled with the hypothesis of continuous degradation rate variation along the polarization curve and is proportional to the flow of protons through the membrane and the catalysts.

In the literature, it is a common practice to consider the V_{FC} as the parameter indicating the load of the FC system. However, the voltage of FC stacks is a consequence of many factors such as the cathode/anode conditions, the stack temperature, and, mainly, the current density which defines the flow of protons going through the membrane, the amount of H_2 dissociated at the anode catalyst layer and the reaction rate of water formation at the cathode catalyst layer. As a consequence, it seems more correct to consider the current density as the variable defining the FC load and the influence of the electrochemical phenomena on degradation rates. In this model, the algorithms were based on detecting the current density and the voltage-based data in the literature was converted to current-density-dependant data using empirical data for the developed model [10].

The phenomena modeled in each layer and a detailed description of the equations above is performed in Section 3.3.1. The 1st layer is described by the reference values $\delta_{x,ref}$ obtained from experimental degradation test procedures, the 2nd is described by the ξ functions which represent the normalized scaling function of the degradation rate with the operating conditions by considering the electrochemical nature of FC degradation, and the 3rd layer is described by the τ and η functions representing the rate of change of the degradation phenomena with temperature and relative humidity. The voltage degradation

described in the above equations is applied over a reference current density (i_{ref}) and then spread along the polarization curve as explained in Section 3.3.5.

3.3.1. Degradation model overall structure

As described in Section 3.3, the model architecture consists of 3 different layers, being the 1st layer composed by experimental degradation rates measured at very specific conditions while the 2nd and the 3rd layers are used to scale-up or scale-down the reference degradation rates. In this section, each layer of the model is explained and the equations used to scale the degradation rates are described. Note that all the scaled degradation rates are defined as the degraded voltage value over the non-degraded FC voltage and that they are applied over a reference current density of 1 A/cm^2, in line with DOE 2020 targets for PEMFC durability [55].

The distribution of the voltage loss along the polarization curve, which is not constant, is not included in this section since it is not something affecting the degradation rates but an implementation strategy. As such, even though it is part of the model structure and could be considered a 4th layer, it was separated and explained in Section 3.3.5.

Note that all the experimental data used in this study were retrieved from different sources in the literature. As such, each figure and table has in the title a reference for the study used to retrieve the data.

3.3.2. 1st layer: reference degradation rates

The 1st layer of the model contains the reference degradation rates, which must be expressed as a fraction or % of voltage loss as a function of the time under a certain condition (low-power or high-power) or per number of cycles (load-changing or start–stop). These degradation rates would correspond to those that should be obtained from reference durability testing protocols, under controlled conditions of T_{FC} and RH. Note that it is imperative to know the values of the reference conditions during the test so that the scaling functions of the 2nd and the 3rd layer are calibrated to be 1 at these conditions. In particular, the degradation rates used in this model were obtained from experimental laboratory tests (Table 1) [28,29]. These degradation tests were performed at $T_{FC} \sim 50$ °C and $\overline{RH} \sim 80\%$ and their results have been widely used in the literature [30–33,56], although they are used as constant degradation rates without considering how they should change with the FC stack operating conditions. This may induce some error in the actual degradation rate prediction since the T_{FC} and $\overline{RH}$ of the FC stack deviates significantly from those values during driving cycle conditions. In addition, these degradation rates were measured at 1 A/cm^2 (corresponding to ~0.7 V in the considered FC system [10]) for the high-power condition, at 0.01 A/cm^2 for the low-power condition and with a load-change cycling amplitude going from the low-power to the high-power condition.

Note that, in this study, the coefficient for the high-power condition was adjusted with respect to their original value in [28] after the model calibration since the experimental data model from which these reference degradation rates were obtained did not consider any natural degradation. This means that the steady-state natural degradation should be included into the steady-state measurements of the degradation rate at low-power and high-power condition in [28]. As a consequence, the reference degradation rates for these conditions were overestimated and should be recalibrated to the values in Table 1 to allow the inclusion of PEMFC natural degradation.

The degradation rates in Table 1 were used in this model for calibration and validation purposes. The model was built in such a way that these coefficients could be changed by state-of-the-art degradation rate coefficients to update the model to represent the degradation behavior of contemporary PEMFC technology. In order to do so, the testing conditions at which the new degradation coefficients were obtained should be known and the scaling functions $\tau(T_{FC})$ and $\eta(\overline{RH})$ adjusted so that their value is 1 at those conditions.

Table 1
Reference degradation rates (1st layer) to be scaled.

Condition	δ [fraction V loss]
Low power [/h] $\left(\frac{d\delta}{dt}\Big\vert_{lp,ref}\right)$	$1.26{\cdot}10^{-5}$
Load change [/cycle] $\left(\frac{d\delta}{dn_{lc}}\Big\vert_{ref}\right)$	$5.93{\cdot}10^{-7}$
High power [/h] $\left(\frac{d\delta}{dt}\Big\vert_{hp,ref}\right)$	$1.03{\cdot}10^{-5}$
Start–stop [/cycle] $\left(\frac{d\delta}{dn_{ss}}\Big\vert_{ref}\right)$	$1.96{\cdot}10^{-5}$

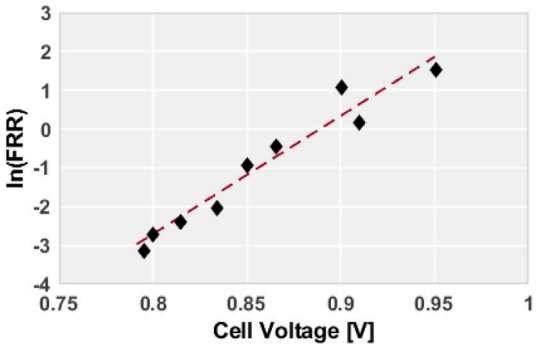

Fig. 5. Fluoride release rate evolution with cell potential.
Source: Data adapted from [61].

3.3.3. 2nd layer: electrochemical phenomena

The 2nd layer is used to be able to use the degradation rates measured at a specific current density (low-power and high-power) or current density cycle amplitude (load-change) along the polarization curve by scaling them with the main electrochemical degradation-related phenomena and how they are affected by the FC operating condition (physical trends). In this section, the origin and expressions of ξ_{lp}, ξ_{lc} and ξ_{hp} are described.

3.3.3.1. Low-power/idle condition. PEMFC stack degradation is mainly due to membrane and cathode degradation. Membrane degradation rate can be quantified through fluoride release rate (FRR), affecting the membrane chemical composition through the decrease in the fluoride concentration and thus the membrane ionic conductivity [57,58]. Catalyst degradation has a direct effect on the electrochemical surface area (ECSA) and the effective platinum surface area (EPSA), thus affecting PEMFC performance through the increase in the activation losses [59], being the decrease in performance due to ECSA loss more significant than that due to membrane degradation [60].

The operation at low current densities implies high voltages (significant from >0.8 V), which is translated into increased electrochemical energy for degradation mechanisms. Under this condition, at steady-state operation, the FRR was detected to increase with voltage, i.e., decrease with current density [61]. This trend is represented in Fig. 5 and shows how the membrane degradation rate varies with the FC load.

At this condition, general surface carbon oxidation affects the catalyst, the gas diffusion layer, and the bipolar plates material, having a noticeable effect on PEMFC performance. This performance decay was identified by measuring anodic peak currents following the cyclic voltammetry methodology after holding the PEMFC at 0.8, 1, and 1.2 V for a certain period of time by Kangasniemi et al. [62]. Since the increase in the anodic peak current is directly related to the PEMFC performance decay, it is also indicative of the increase in the degradation rate.

The data shows the membrane [61] and catalysts [62] degradation phenomena was converted to current-density-dependent, weighted considering that 20% of the degradation is produced in the membrane and 80% in the catalyst, and normalized so that the combined scaling function has a value of 1 at 0.01 A/cm^2, where the low-power degradation

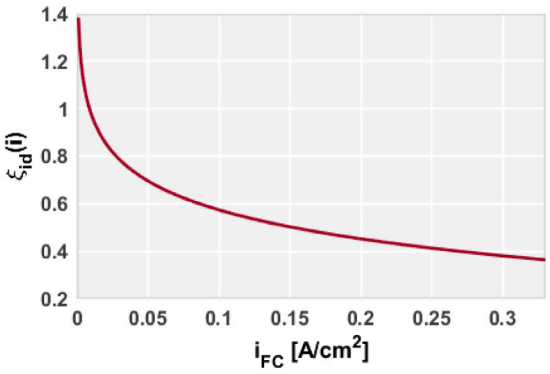

Fig. 6. ξ_{lp} evolution with current density.

rate was measured. As a result, the normalized scaling function $\xi_{lp}(i)$ was defined as:

$$\xi_{lp}(i) = -0.176 \cdot \ln i + 0.169 \tag{17}$$

Note that this scaling function, represented in Fig. 6, is only valid on low-power conditions, i.e., when $i < i_{lp}$. When the PEMFC is operating in other conditions the value of this function becomes 0 to deactivate the degradation mechanisms belonging to the low current density operation. The threshold i_{lp} is calibrated on Section 3.3.6 to identify the boundaries on which each degradation mechanism dominates the PEMFC aging based on experimental data.

3.3.3.2. Load-change condition. The degradation due to load-change condition is mainly due to fast changes in i, T_{FC}, $\overline{RH}$, stoichiometry (λ), ...The main phenomena producing the membrane and catalysts degradation are the problems associated with the anode starvation, flow, and water management. These phenomena are due to the mismatch between the characteristic time of the flow and the characteristic time of the electrochemical and electric phenomena [61]. Knowing this, it is possible to conclude that origin of the load-change degradation is continuous, i.e., it is difficult to quantify it by means of discrete voltage cycles. However, predicting such detailed issues of the FC stack inner flows management is not affordable in the frame of 0D-1D FC models. As a consequence, in those studies where the degradation rate due to the load-change condition is intended to be predicted with 0D-1D FC models, the authors mostly try to detect the current density oscillations (n_{lc}) or the time at which the FC is under the load-change condition without indicating a criterion to identify or scale such load-change condition and apply the corresponding degradation rate at reference testing condition per load-change cycle or unit of time [33,63]. Nevertheless, the voltage oscillations that an FC stack suffers under driving conditions are far from close to those to which FC stacks are subjected on voltage cycling tests (standardized degradation tests). In order to address this discrepancy, a discrete problem such as the voltage cycling was again converted to a continuous degradation problem, close to its actual nature. To do so, this degradation model monitors the variation of the current density each time step.

With only this detection strategy the degradation under load-change conditions is considered again as a continuous phenomenon. Nonetheless, these rules are only useful to detect the presence of the degrading condition, not to quantify the degradation rate at different load-changing cycles. In order to address this issue, it is assumed that the intensity of the degradation phenomena scales with the amplitude of the load change for a given time-step, i.e., with the magnitude of di/dt, from the reference condition. With these hypotheses, the corresponding analytical expression of ξ_{lc} is:

$$\xi_{lc}\left(\frac{di}{dt}\right) = \frac{\frac{dn_{lc}}{dt}\frac{d\delta}{dt}}{\frac{d\delta}{dt}\Big|_{lc,ref}}$$

$$\frac{d\delta}{dt}\Big|_{lc,ref} = \frac{d\delta}{di}\frac{di}{dt}\Big|_{lc,ref} = \frac{d\delta}{di}\frac{di}{dn_{lc}}\Big|_{lc,ref}\frac{dn_{lc}}{dt}$$

$$= \frac{d\delta}{di}\frac{dn_{lc}}{dt}\, 2\,|\Delta i|_{ref}$$

$$\frac{d\delta}{dt} = \frac{d\delta}{di}\frac{di}{dt} = \frac{d\delta}{di}\,|\Delta i|_{dt}$$

where $|\Delta i|_{ref}$ is the reference current density amplitude for the voltage cycling test per voltage cycle (0.99 A/cm^2) and $|\Delta i|_{dt}$ is the absolute value of the current density variation for a given time step dt. Note that $|\Delta i|_{dt}$ is used in absolute value and $|\Delta i|_{ref}$ is multiplied by 2 to account for the FC degradation when increasing (potential starvation) and decreasing (potential water management issues) the current density in voltage cycling tests and driving cycle conditions. The term dn_{lc}/dt is included in ξ_{lc} to convert the discrete voltage degradation rate at reference conditions ($d\delta/dn_{lc}|_{ref}$) to a continuous degradation rate that depends on time. Deriving the above equation, the final expression for ξ_{lc} is:

$$\xi_{lc}\left(\frac{di}{dt}\right) = \frac{dn_{lc}}{dt}\frac{\frac{d\delta}{dt}}{\frac{d\delta}{dt}\Big|_{lc,ref}} = \frac{|\Delta i|_{dt}}{2\,|\Delta i|_{ref}} \tag{18}$$

3.3.3.3. High-power condition. FC stack degradation mechanisms are generally less relevant at high-power conditions than at low-power or load-change conditions. However, in high-power conditions, the ohmic and electrochemical losses of the FC stack are high, which increases the heating of the FC stack. The increase in T_{FC} at this condition may increase the intensity of the degradation phenomena, thus potentially resulting in higher degradation rates than at low-power conditions. The degradation phenomena that are intrinsic of the high-power condition are the appearance of partial oxygen starvation, high membrane water content (accelerates oxidation and corrosion mechanisms), and a general increase of the kinetic, ohmic, and mass transport losses. All these phenomena only occur from a certain current density and scale with the flow of protons through the membrane, which is directly proportional to the current density under normal operation. As such, the degradation mechanism at high-power conditions without considering the independent effect of T_{FC} and $\overline{RH}$ should scale with the current density:

$$\xi_{hp} = \frac{i}{i_{hp}} \tag{19}$$

where i_{hp} is the minimum current density at which the high-power degradation becomes significant (calibrated to experimental data to 1 A/cm^2). This scaling function (ξ_{hp}) has a value of 0 when $i < i_{hp}$, thus activating the high-power degradation diagnosis only at high-power condition.

3.3.3.4. Medium-power/natural degradation. Natural degradation in FC is usually used in the literature to model the natural decay of the FC stack components during the steady-state or low-dynamics operation. These degradation phenomena are relevant, especially for the FC that is used for power generation but simply a small fraction of the total degradation for FC that operate under dynamic conditions, such as those for transport application. As commented before, this model considers the natural degradation to be independent conditions of T_{FC} and $\overline{RH}$ but proportional to the flow of protons through the membrane and the catalysts, i.e., to the current density (Eq. (15)). Natural degradation is often modeled as a constant voltage decay with time since it is extremely time and resources consuming to measure [64]. As a consequence, natural degradation rates are only measured at a specific current density, so the effect of changing the current density on natural degradation on the same FC type and under the same conditions is unknown. However, it is expected that the FC natural decay scales with the rate at which the electrochemical phenomena are taking place in the membrane and

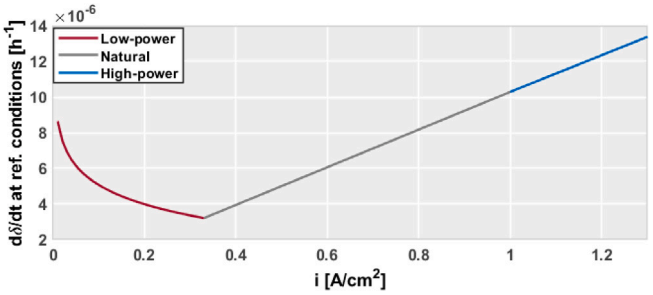

Fig. 7. Evolution of dδ/dt at reference conditions of T_{FC} and $\overline{RH}$.

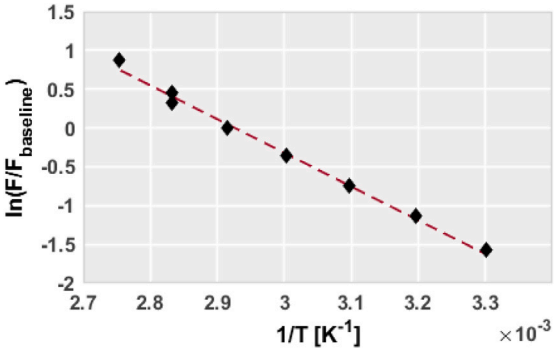

Fig. 8. Fluoride release rate relationship with temperature using DuPont Nafion® 112. *Source:* Data retrieved from [61].

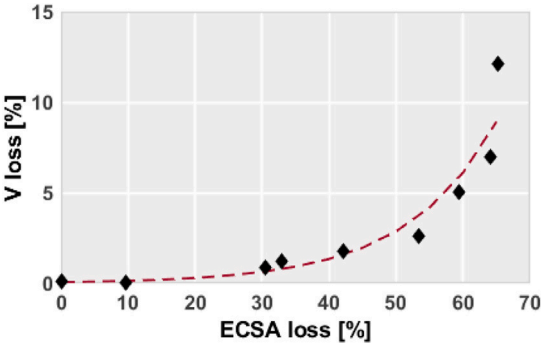

Fig. 9. Correlation between V loss [%] and ECSA loss [%] approximated from data from [61,68] by measurements at 1 A/cm^2 after voltage cycling tests.

the catalyst. This effect was included in this model as in Eq. (15) and was checked in the validation section so that it implies steady-state degradation rates that offer ~40000 h until the end of life, in line with DOE 2020 targets [54]. This implementation strategy implies that the degradation rate at reference conditions is continuous (Fig. 7) and that part of it is included in the low-load and high-power conditions. In fact, with this hypothesis, high-power degradation is mostly natural degradation enhanced with the flow of protons through the membrane.

3.3.4. 3rd layer: physical conditions

Once the reference degradation rates are scaled with the electrochemical phenomena, they must be scaled with the physical conditions in the FC stack. Among the different conditions that affect the PEMFC stack degradation rates, the stack temperature (T_{FC}) and the membrane relative humidity have the most significant effect through the increase of the reaction rate of the degradation-associated chemical reaction and the change in the cathode catalyst layer properties (Pr grain, size, thickness, and carbon corrosion). In this model, the average value of the relative humidity between the anode and the cathode ($\overline{RH}$) was chosen instead of the membrane relative humidity since it is not measurable and depends on other submodels that may induce additional errors. The approach of considering the average RH is in line with the extended method of calculating the membrane water content, which is predicted assuming equilibrium from the activity of the vapor phase of the inlet flows/relative humidity (RH = $X_{H_2O} \cdot p/p_{sat}$) [24,65] as the average of the water content between the anode and the cathode catalyst layers [66]. Selecting locally the anode or the cathode relative humidity at the stack inlet would indeed make the degradation results depend significantly on the anode/cathode humidifying strategy, which may differ from the actual conditions of water content at the membrane and catalysts that are affected by the water production at the cathode catalyst layer which is accounted for in the RH at the anode and the cathode through solving the mass transport equation. The fact of considering $\overline{RH}$ helps on the applicability since it is a measurable parameter and can be obtained from simulations.

3.3.4.1. Temperature effect on degradation. The effect of temperature on degradation rate is defined by the $\tau(T_{FC})$ function and is common to all the degradation rates at different conditions. Operation temperature has the strongest influence on the degradation mechanisms and the FC contamination. Analogous to the effect of low-power condition over degradation, this model considers the effect of T_{FC} over membrane and cathode catalyst degradation mechanisms. In the case of membrane degradation, it is due to chemical mechanisms that produce non-zero fluoride release rates and follows an Arrhenius relationship with temperature (Fig. 8).

In the case of the catalyst degradation, the operating temperature has a direct effect on the ECSA, i.e., Pt surface loss, through Pt dissolution and grain growth. This model uses the data obtained by Bi et al. [67] at 40, 60, and 80 °C where the remaining ECSA was measured after 110 h of potential cycling tests (46, 29, and 26% respectively). This remaining ECSA was then converted to equivalent V loss by relating the ECSA loss to V loss at 1 A/cm^2 under voltage cycling tests from 0.6 V to 1.3 V from the experimental data obtained by Jia et al. [61,68] with the following equation (Fig. 9):

$$V_{loss}\ [\%] = 0.06447 e^{0.0758 \cdot ECSA_{loss}\ [\%]} \tag{20}$$

The voltage loss derived from the catalyst degradation and the fluoride release rate was normalized so that their value is 1 at reference temperature (50 °C) and combined assuming that 20% of degradation comes from the membrane and 80% from the catalyst degradation mechanisms. From this data, the function that scales the degradation phenomena with the stack temperature is defined as:

$$\tau(T_{FC}) = -5.390 \cdot 10^{-4} T_{FC}^2 + 0.399 \cdot T_{FC} - 71.576 \tag{21}$$

being it valid in the range of $T_{FC} \in [310, 373.15]$ K.

3.3.4.2. Relative humidity effect on degradation. High relative humidity conditions have significant effects on electrode degradation. Namely, high RH affects the catalyst layers by enhancing the degradation mechanism associated with Pt grain growth [69], Pt loss, [70] and cathode catalyst layer (CCL) thickness [71]. Among these three parameters, the ECSA degradation rate is mainly affected by the Pt grain size growth. In order to characterize the effect of RH on Pt grain size growth rate, the same voltage cycling test was performed under different conditions of RH by [71] (Fig. 10). From these results, it was possible to identify the negative impact of RH on electrode assembly degradation. Nonetheless, to apply these results to the current model, it is necessary to translate them into an equivalent decrease of ECSA, then to equivalent voltage loss, and finally to normalize them into a function $\eta(\overline{RH})$ whose value is 1 at reference conditions ($\overline{RH}$ = 80%). The relation between the ECSA and the radius of the Pt gran in the catalyst layer (r_{Pt}) is [41]:

$$ECSA = \epsilon_1 \frac{3}{r_{Pt} \rho_{Pt}} \tag{22}$$

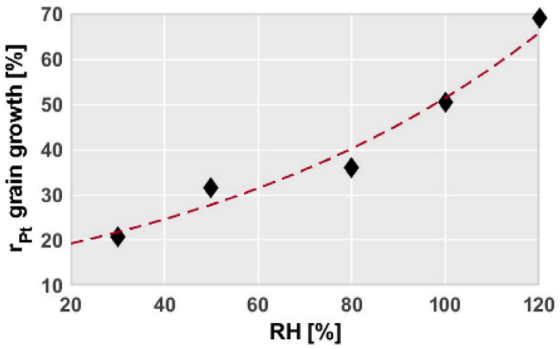

Fig. 10. Evolution of catalyst Pt grain size growth after 3000 voltage cycles.
Source: Data extracted from [61,71].

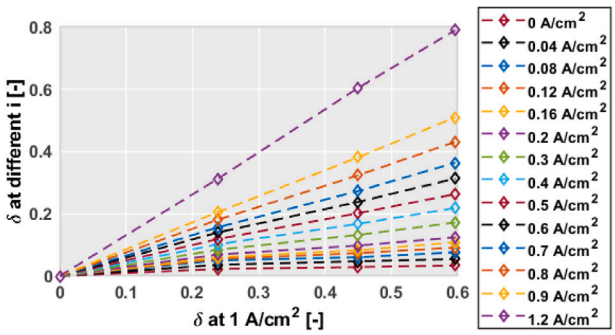

Fig. 11. Relation between voltage loss δ at reference current density and δ along the polarization curve.
Source: Data extracted from [73].

where ρ_{Pt} is the Pt density. Note that ϵ_1 and ρ_{Pt} are constant parameters. Therefore, the decrease in ECSA is inversely proportional to the increase in Pt grain size growth.

The remaining ECSA is then computed from the data in Fig. 10 and Eq. (22). Finally, $\eta(\overline{RH})$ is obtained by converting the ECSA loss into voltage loss through Eq. (20) and normalizing the resulting function so that it is 1 at $\overline{RH} = 80\%$:

$$\eta(\overline{RH}) = 0.10646e^{0.028 \cdot RH \ [\%]} \tag{23}$$

This equation is valid for RH up to 100% since membrane flooding and its effect on degradation is not within the scope of this model and it usually does not happen during normal operation if the flows are managed properly. For RH higher than 100%, it is expected that other degradation mechanisms, such as gas diffusion layer wear or enhanced catalyst corrosion [72], increase the degradation rate

3.3.5. Degradation model integration

3.3.5.1. Integration along the PEMFC polarization curve. As it is commonly known, the voltage along the polarization curve of an FC changes with the current density depending on the activation ohmic, concentration, and internal current losses. As a consequence, applying a certain ΔV or δ due to degradation over two different current densities has different effects on the FC performance. In most of the studies in the literature, the degradation effect is assumed to be uniformly distributed along the polarization curve, which has been proved not to be the case [73]. In order to address this issue and to provide a more faithful and physical distribution of the degradation effect over the polarization curve, this model was designed to calculate all the degradation rates (Section 3.3.1) as the voltage loss over a reference current density of 1 A/cm^2 and then spread the voltage loss along the polarization curve from experimental results.

The data used for this purpose was that found in [73]. In this study, Bezmalinovic et al. performed accelerated stress voltage cycling tests over a PEMFC and measured the polarization curve before the tests, and after 1000, 3000, and 5000 cycles. From these experimental polarization curves, it was possible to identify how the polarization curve (voltage) changes at each current density at different degradation states.

In order to spread the degradation effect from the model reference current density (1 A/cm^2) to different operating points, the variation of the voltage at each current density of the experimental polarization curve in [73] was compared against the voltage variation at the reference current density (Fig. 11). From this comparison, it was concluded that the variation of the voltage due to degradation at any current density varied linearly with the voltage degradation at the reference current density of 1 A/cm^2. As such, the experimental data in Fig. 11 was used to spread the value of δ along the polarization curve. Note that this data also accounts for very advanced degradation states where the PEMFC has already reached the end of life.

3.3.5.2. Integration with PEMFC models. As explained before in Section 3.3, this model was designed to be a plug-in model in any PEMFC simulation environment. Two different approaches could be followed in order to integrate this properly into a FC model, depending on the FC control strategy.

In the first case, if the FC control is performed by means of power demand, the variable δ at the corresponding current density for each time step could be applied directly over the electrical power of the FC as a power-decreasing factor:

$$P_{FC,deg} = P_{FC} \cdot (1 - \delta) \tag{24}$$

Note that, in this case, the system controller should be aware of the power deficit due to degradation and adjust continuously the current density to match the power demand considering the degradation effects. This approach is useful to understand the power decrease and perform estimations over the increase in H_2 consumption due to the degradation state. Nonetheless, the EMS is not aware of the degradation effects over the power production capabilities of the PEMFC.

The second approach is useful, especially in dynamic simulations such as driving cycles where the energy flows should be properly managed to achieve the optimum global efficiency. It consists of integrating this model both in the PEMFC and into the EMS in such a way that the EMS optimizer is fully aware of the real H_2 consumption and power production capability at each current density. In this case, the internal and simple PEMFC models that the EMS usually have should have integrated this degradation model and used it to modify the decision space. The value of δ could be applied over the voltage or over the FC electrical power. Although this approach implies some duplicity, it is recommended since only implementing the degradation effects on the PEMFC model but not in the EMS would produce some mismatch between the models, inducing numeric errors.

3.3.6. Validation

The validation of the model was performed with the data in [28], considering the simulation of a FC bus operating in real driving cycle conditions. Fig. 12 describes the power demand of the FC under real driving conditions measured experimentally from a city bus operating on a daily route. To perform the validation of the model, a validated FC system model developed on the software GT-Suite was used following previous studies [11]. This model was modified to have the same characteristics as the FC stack in the bus (280 cm^2 of active surface area and similar power output). This stack was then integrated into a balance of plant so that the flow conditions of the FC stack were representative of those in an FCV.

After simulating this driving cycle and obtaining the evolution of the current density, the temperature, and the cathode and anode relative humidity, the degradation rates by source were compared (Fig. 13). The experimental data obtained by Pei et al. included two different degradation sources on steady-state conditions (low-power/idle

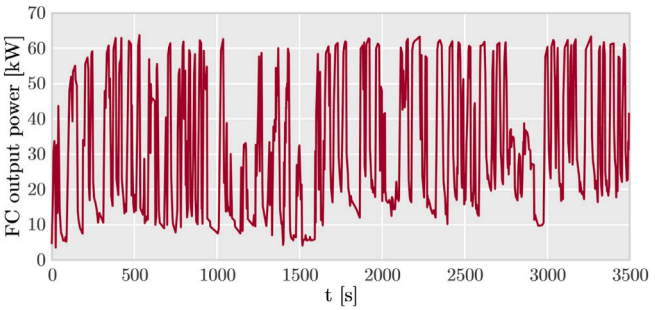

Fig. 12. FC stack power demand under the real driving cycle used for validation, retrieved from [28,29].

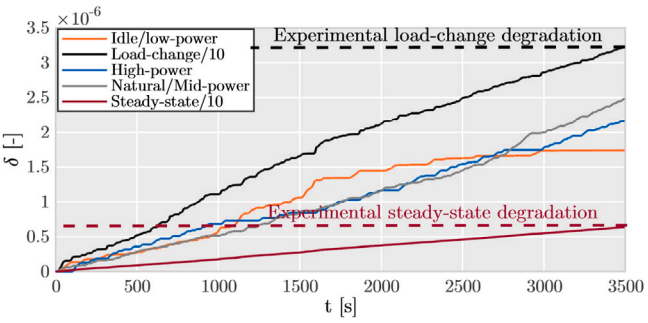

Fig. 13. Validation results: comparison of experimental [28] degradation rate sources at the end of the driving operation in Fig. 12 with model degradation rate sources. Steady-state degradation comprises low-power, high-power, and natural (medium-power) degradation. Load-change and steady-state voltage loss ratio (δ) evolution were divided by 10 to improve readability.

and high-power conditions) but did not take into account the natural degradation rate of the FC stack. As such, the experimental data they provided that accounted for the steady-state degradation must have implicitly included the natural degradation. The validation approach in this paper consists of matching the degradation coming from load-changing cycling and steady-state operation to the corresponding experimental data. In this sense, the sum of the low-power, high-power, and natural degradation in the model should correspond to the sum of the low-power and high-power degradation experimental data, denoted as *Experimental steady-state degradation* in Fig. 13. As the last step, the degradation rate coming from the natural degradation mechanism was checked to be consistent with the usual life of PEMFC operating under steady-state operation. Note that the start–stop degradation rate, expressed as a function of the number of start–stop cycles, was set to the same value as in the experimental data provided by Pei et al. [28] (see Table 1).

Fig. 13 shows the evolution of the degradation state by source compared to the experimental degradation predicted by Pei et al. [28] at the end of the bus operation based on the relative breakdown of the degradation rate sources. From the data in this figure, compared to the FC output power evolution in Fig. 12, it is possible to understand how the model reacts properly to the FC operation, i.e., the degradation due to load-change increases with changes in the FC output power and is the highest source of degradation, low-power/idle degradation increases more in the first half of the operation in which the power reaches lower values and slows down after 1600 s, and natural and high-power degradation increase almost constantly due to the frequent load changes during the bus operation. Some time intervals, such as 1000 s to 1250 s, show how high-power degradation does not increase when the FC model does not operate under high-load conditions. This is also perceived, for example, from 3000 s where low-power degradation remains constant (degradation rate due to low-power operation is 0).

In order to calibrate the model to approach the experimental results, the model parameters i_{lp} and i_{hp}, defining the border between different degradation conditions (Fig. 7), were calibrated in such a way that the error in the degradation rate for each power source is lower than 0.1%. The calibrated values of i_{lp} and i_{hp} are 0.33 A/cm^2 and 1 A/cm^2 respectively. These two parameters have been selected as the calibration parameters since they correspond to the maximum current density for which the low-power/idle degradation mechanism is considered (i_{lp}) and the minimum current density for which high-power degradation is accounted for (i_{hp}). As such, they define the range of current densities in which the scaling functions $\xi_{lp}(i)$ and $\xi_{hp}(i)$ are non-zero, and the variation of the natural degradation with the current density.

Finally, in order to identify whether the natural degradation rate was modeled properly, the total life of the PEMFC stack due to only the natural degradation was calculated assuming the end of life when $\delta = 0.1$ at 1 A/cm^2. In the validation case, degradation rate due to natural degradation was $2.57 \cdot 10^{-4}$ % V loss/h, which implies a life of ~39600 h, in line with DOE 2020 targets [16].

4. Effect of sizing and dynamic limitations over performance and degradation

4.1. Effect over the FC system behavior

In consistency with previous studies [10], the current density evolution along the driving cycle is expected to vary when modifying the FC maximum power through the number of cells and the dynamic response of the FC system. As such, and given the importance of the FC system operation on degradation and performance, it is important to understand and analyze the FC behavior and how it changes when acting over any of these parameters. For that purpose, Fig. 14 shows the current density evolution change for the 40 kW and 100 kW FC maximum power designs under dynamic restrictions ranging from 0.001 A/cm^{2}s (extremely high restriction) to 1 A/cm^{2}s (almost infinite dynamics). Although the 60 kW and 80 kW designs were also included in the analysis, their current density evolution is not represented in Fig. 14 to improve the readability and simplicity of the graphs. In contrast, the highest-power and lowest-power designs were used to highlight the effect of FC stack sizing. This figure is used to complement the results in Figs. 15 and 18 showing the H_2 consumption and degradation rate change.

The selection of the dynamic restrictions to 1, 0.1, 0.01, and 0.001 A/cm^2 was motivated by the different scenarios they represent. The first value represents the case of almost infinite dynamics since during the simulation of the FCV in WLTC 3b cycles without any dynamic restriction the $|di/dt|$ was mostly below 1. The second value (0.01 A/cm^2) was established as a dynamic limit representative of high dynamics by with a certain limitation to prevent cathode/anode starvation since the stoichiometries were more stable and closer to the target values while preserving the highly-dynamic operation. The case with 0.001 A/cm^2 (extreme dynamics restrictions) represents the case of the expected operation of a range-extender (not the actual one) in which the power demand oscillations are slow (see Fig. 14, graph D). This represents the dynamic limit under which the condition imposed in the EMS of keeping the battery SOC at the same value at the beginning and the end of the driving cycle is not fulfilled in aggressive driving patterns (estimated by considering the ARTEMIS Motorway driving cycle). Finally, the restriction of 0.01 A/cm^2 is a value in between the high and low dynamics (moderate dynamics) that allows the FC reach high current densities while limiting the intensity and the amplitude of load-changing cycles (see Fig. 14, graph C).

The effect on the current density evolution of FC stack sizing can be analyzed with the data in Fig. 14.A, where the dynamic limitation is negligible and the FC system operates close to the optimum behavior to minimize H_2 consumption since the EMS is not constrained by the FC dynamics. In contrast, given the importance of load-change degradation

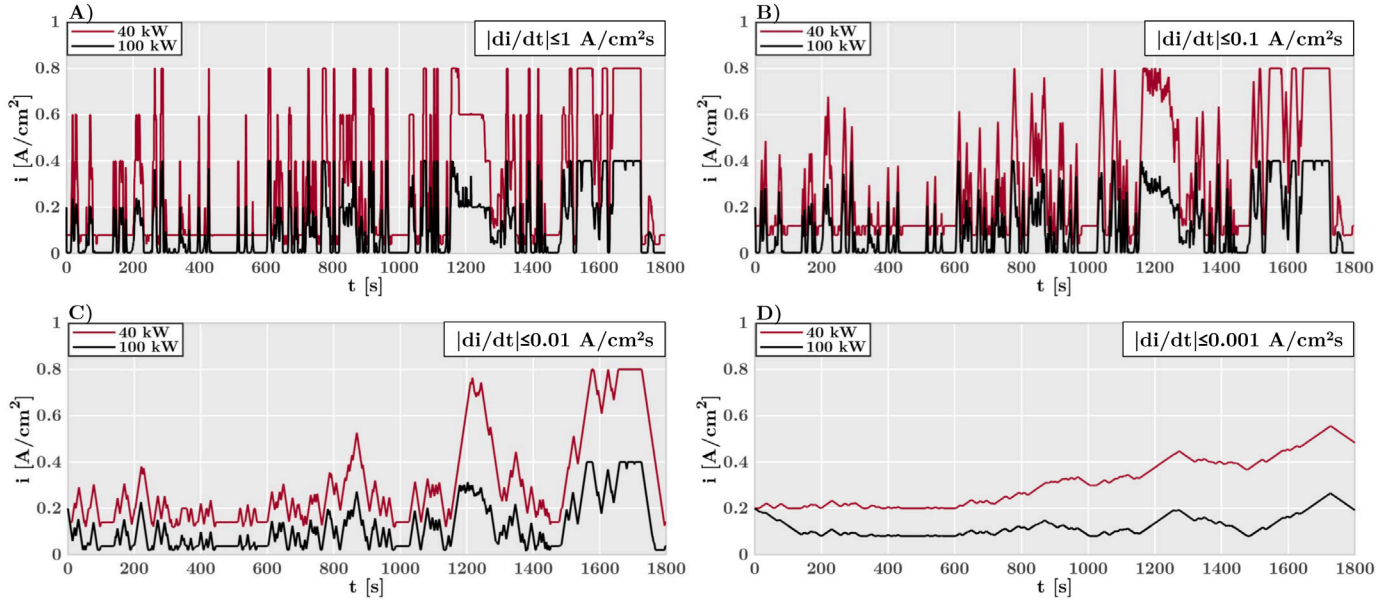

Fig. 14. Current density evolution along WLTC 3b driving cycle for 40 kW and 100 kW FC stack maximum power with dynamic limitations ranging from 0.001 A/cm^2 to 1 A/cm^2.

in driving cycle conditions, FC durability is expected to be lower compared to other cases with lower dynamics. An overall decrease in current density is perceived when increasing the FC maximum power. This is motivated by the fact that an FC stack with a high number of cells (100 kW) operating at a certain current density produces more power than a stack with a lower number of cells (40 kW) at the same current density. Therefore, since both FCV designs are being used in the same driving cycle (WLTC 3b) the power demand by the electric motor will be similar, provided that it increases slightly for the case of the 100 kW FC stack design due to the higher powertrain weight. Lower H_2 consumption is expected for the 100 kW design since it operates at lower current densities, which implies higher FC system efficiency. Interestingly, the maximum current density along the cycle for the 40 kW design is 0.8 A/cm^2 while it is 0.4 A/cm^2 for the 100 kW although the number of cells increases by a factor of 2.5. This happens since the energy management strategy optimizer that minimizes H_2 consumption prevents the 40 kW stack to operate at the lowest efficiency region, i.e., at high current density (>0.8 A/cm^2). Instead, to compensate for the lack of power provided by the 40 kW FC when the e-motor power demand is high and fulfills the charge sustained condition, the minimum current density increases compared to the 100 kW design.

Increasing the FC dynamic limitation to 0.1 A/cm^{2}s (Fig. 14.B) does not produce significant changes in the current density distribution since the limitation is still low and allows for high dynamic behavior. Nevertheless, some changes in both the 40 kW and the 100 kW designs can be perceived at the high current density peaks and in the minimum current density. In this sense, due to the dynamic restrictions, some peaks in Fig. 14.A with a value of 0.8 A/cm^2 for the 40 kW design cannot be reached in Fig. 14.B, meaning that the operation, in terms of minimizing H_2, is suboptimum. In order to compensate for this local lack of power supplied by the FC and keep the charge sustaining mode, the minimum current density increases, thus providing more power along the driving cycle. These changes are more noticeable for the 40 kW design but are also present, although to a lower extent, for the 100 kW design. Given the current density evolution in Fig. 14.B, some penalty in terms of H_2 consumption and some benefit in terms of durability could be expected. Nonetheless, the effect in both parameters should be low since the dynamic limitation is not significant.

When the dynamics are noticeably limited to values of 0.01 A/cm^{2}s and 0.001 A/cm^{2}s (Figs. 14.C and 14.D, respectively), the current density evolution along the cycle changes significantly and has important effects on both H_2 consumption and FC stack durability are expected. In the case of Fig. 14.C, both designs suffer an increase in the minimum current density to compensate for the suboptimum operation and the maximum current density is used less often, which will result in a significant penalty on H_2 consumption. This may imply an overall decrease in medium-power or natural degradation, followed by a decrease in low-power or idle degradation due to high-potential cell values. Furthermore, load-change intensity is clearly affected. Therefore, an overall decrease in the total degradation rate should be expected since the major source of degradation (load-change) is directly acted on. Nonetheless, the increase in the minimum current density also implies an increase in the rejected heat of the FC along the cycle, thus an increase in the FC stack temperature and a potential increase in all the degradation sources. The resulting degradation rate will consist of a trade-off between these effects.

The case with the highest dynamic restriction (Fig. 14.D) offers a smooth current density evolution along the driving cycle. In this case, for both designs, a decrease in the maximum current density, an increase in the minimum current density, and a decrease in the load-change cycle intensity and amplitude is perceived. Following the same reasoning as with the case in Fig. 14.C, degradation rate should decrease and H_2 consumption should increase significantly, but the effect over durability should be determined taking into account the FC stack physical conditions, not only the current density evolution. Nevertheless, this highly-restricted dynamics constraint was tested over different FC stack size designs and driving cycles. From these results, it was determined that high-dynamics restrictions may prevent the controller to fulfill the charge sustaining condition when low-power FC stacks are considered (20–40 kW) in high-power and high-dynamics driving cycles (ARTEMIS Motorway) and that it will significantly depend on the initial current density at the beginning of the cycle. Therefore, this constraint is not recommended for automotive applications since it may limit the flexible operation of FCREx vehicles.

4.2. Effect on FCV performance

The effect of sizing and dynamics limitation on H_2 consumption and FC stack degradation rate can be mostly attributed to the change in the FC current density evolution (Fig. 14). However, it is important to differentiate between the effect of applying dynamic restrictions and the effect of increasing the FC maximum power both in degradation rate (by degradation source) and performance.

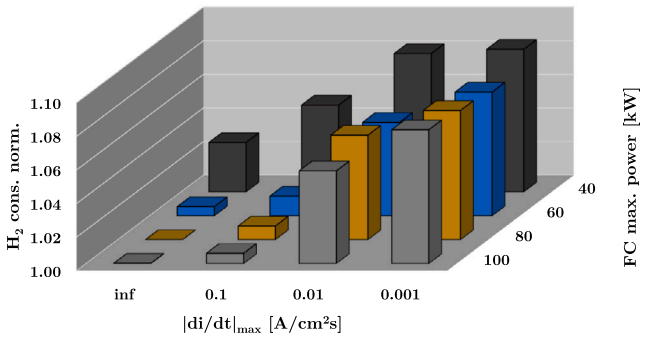

Fig. 15. Normalized H_2 consumption evolution as a function of the FC stack maximum power and the dynamic limitations.

In this section, normalized values are presented since they provide benefits for comparative analyzes. Nonetheless, the absolute value of H_2 consumption is within the expected range of FCV since this model was used in previous studies where it was validated and compared against commercial FCVs [10,11]. The same can be said for degradation rates which, even in the case that the FC technology improves in durability, the tendencies in relative terms should conserve as they are scaled with the trends followed by the electrochemical and physical phenomena.

Fig. 15 shows the normalized H_2 consumption of each design with different restrictions on the current density change rate. As commented in Section 4.1, higher FC maximum power implies lower current density, thus a more efficient operation regardless of the slightly higher load. Therefore, H_2 consumption decreases with increasing FC maximum power, but almost no benefit is perceived when increasing the FC power further from 80 kW since, for the selected vehicle application, this stack already operates at the highest-efficiency current density range. From this value of FC stack power, increasing the number of cells of the stack should not provide significant benefits in terms of H_2 consumption decrease but rather it could increase due to the increasing weight. In this sense, H_2 consumption is 3% higher with the 40 kW FC stack compared to the 100 kW design when no dynamic limitation is imposed. In contrast, with a constant FCV design, increasing the dynamic limitation to 0.01 and 0.001 A/cm^{2}s increases H_2 consumption by 5%–8% depending on the design. In the case of the 40 kW design, consumption only increases by 5% (for both 0.01 and 0.001 A/cm^{2}s cases) with respect to its value with infinite dynamics since it is already high without any dynamic limitation. For higher-power FC stack vehicles, there is a noticeable variation in H_2 consumption between the 0.01 A/cm^{2}s and the 0.001 A/cm^{2}s since, differently from the 40 kW design, the 0.01 A/cm^{2}s case allows for higher dynamics in terms of power variation rate, thus decreasing H^2 consumption and suffering higher penalties when increasing the limitation.

4.3. Effect on FC stack durability

As with H_2 consumption, the results obtained from the simulations show how the effect on the durability of varying the FC maximum power is different from that perceived when imposing dynamic limitations on the control strategy. Figs. 16 and 17 show the evolution of the relative weight of each degradation source for different designs and dynamic limitations. These data, together with those in Fig. 18 are useful to understand the change in durability between different designs and dynamic limitations as well as the specific effect of varying the FC maximum power or imposing dynamic limitations on each degradation source. Life was calculated following the end of life (EOL) criteria established by the Department of Energy through which an FC stack is considered to have reached the EOL when the voltage decreases by 10% with respect to nominal conditions at a current density of 1 A/cm^2 [55].

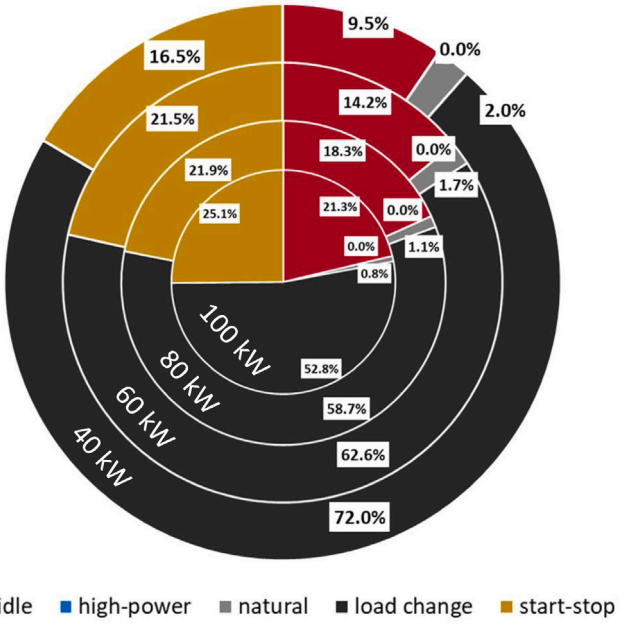

Fig. 16. Degradation source relative effect on FC stack durability decrease for the 40, 60, 80, and 100 kW designs.

The direct effect on the current density evolution change when increasing the FC stack maximum power (Fig. 14) and the decrease in FC stack temperature due to the lower electrochemical losses when operating at low current density produces the increase in FC stack durability with infinite dynamics shown in Fig. 18. This implies an increase in FC durability of 53% when comparing the 40 kW and the 100 kW designs. The detail on how the degradation rate by source change with this design parameter (Fig. 16) shows how load-change degradation, responsible for 72% of the total degradation rate with the 40 kW design, decreases below 53% of total degradation due to the lower load-change cycle amplitude (Fig. 14.A). Star-stop cycling remains the second major source of degradation for all the designs and its relative impact increases as it is constant and does not depend on the FC behavior along the driving cycle (only 1 start–stop cycle was considered per cycle) since it depends mainly on the start–stop sequence and the FC stack technology. As the FC stack's maximum power increases, low-power degradation becomes more relevant while medium-power or natural degradation decreases since the FC stack needs to operate at lower current densities to cover the same power demand.

Imposing dynamic limitations has become a common practice to minimize degradation in FC stacks for automotive applications since load-change degradation is the major source of degradation in this technology. As such, the largest durability increase is perceived when imposing dynamic limitations over the current density change rate rather than when increasing the FC maximum power (Fig. 18), with a maximum increase in FC durability of 294% and 123% for the 40 kW and the 100 kW comparing the infinite dynamics with the highest dynamic restriction cases, respectively. Nonetheless, similar durability is perceived for all the designs when high dynamic limitations are imposed over the FC control (0.01 A/cm^{2}s and 0.001 A/cm^{2}s), meaning that the benefit in the durability of operating under lower current density and lower load-change cycle amplitude cancels out when the load-change intensity (dynamics) is limited. The significant increase in durability is mainly due to the decrease in load-change degradation that varies from 62.6% to 6.9% of total degradation in the case of the 60 kW design (Fig. 17). This decrease in load-change degradation implies a noticeable increase in the relevance of other degradation sources. Start–stop degradation might become the highest degradation source, followed by low-power degradation prior to load-change degradation.

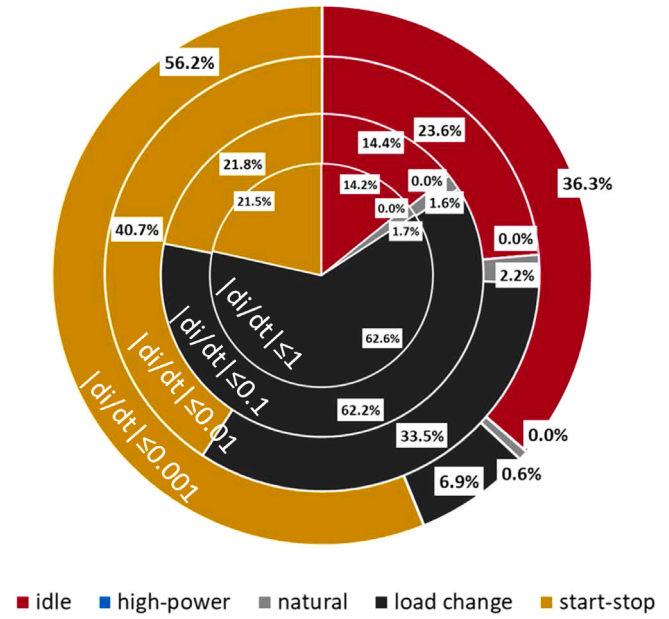

Fig. 17. Degradation source relative effect on FC stack durability decrease for the 60 kW design with different dynamic limitations.

4.4. Industry applied value

The change in the relevance of the degradation source may be important information for FC stack manufacturers for FCREx vehicles with dynamic restrictions since they could focus their research and development efforts in minimizing star-stop or low-power degradation through start–stop sequence or materials improvement rather than on improving the internal geometry of the FC stack channels to improve water management to minimize load-change degradation. This shift could allow higher FC stack durability for FCREx stacks with lower costs provided that the control strategy of the vehicle is designed properly.

In light of these results, vehicle manufacturers should take into account the different implications of increasing the FC stack power and imposing dynamic limitations during the vehicle design phase. Increasing the FC stack power implies lower H_2 consumption (↓ OPEX), higher production costs (↑ CAPEX) [10] and higher FC stack durability. In contrast, increasing the dynamic limitations implies higher H_2 consumption (↑ OPEX), equal production costs (= CAPEX), and higher durability. Vehicle manufacturers should then find a trade-off to minimize costs with sufficient FC stack durability when considering the vehicle design and should take into account the dynamic limitations on the control strategy, if any, in the FC stack sizing process.

As a last remark, it has been analyzed how H_2 consumption is highly penalized when increasing the dynamic limitations, regardless of the FC stack power. In this line, durability has also increased with imposing dynamic limitation, but high durability is already achieved for the 0.01 A/cm^{2}s limitation. As previously discussed, increasing the dynamic limitation to 0.001 A/cm^{2}s may penalize the FCV's flexibility, preventing the control strategy from keeping the charge sustained mode in aggressive and high-power driving conditions. Therefore, the FCV manufacturers should design the FCV control strategy in such a way that the FC system operation provides durability close to the target expected life for the vehicle since over-restricting the dynamics of the FC stack would imply higher H_2 consumption and could compromise the fulfillment of the charge sustaining mode.

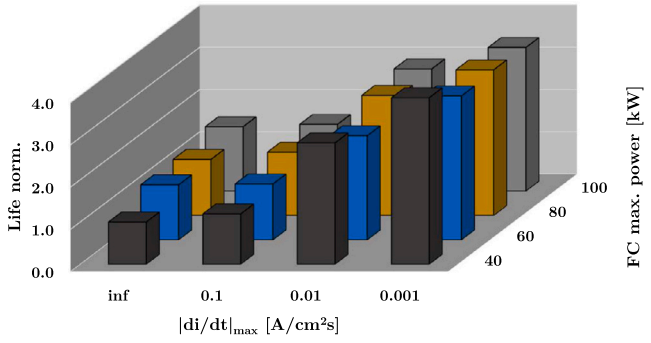

Fig. 18. Normalized FC stack durability (life) evolution as a function of the FC stack maximum power and the dynamic limitations.

5. Conclusion

In this study, a novel semi-empirical multi-layered diagnosis degradation model for PEMFC was developed to understand the effect of FC stack sizing and dynamic limitations on the performance and durability of FCREx vehicles. The modeling approach consisted of scaling the degradation rates obtained from experimental results under controlled and known conditions with scaling functions based on empirical trends representing the change in the PEMFC components degradation due to electrochemical phenomena (i) and physical conditions (T_{FC} and $\overline{RH}$). For that purpose, the model architecture was designed following a multi-layered approach, consisting of 3 layers and a novel degradation effect integration strategy into the polarization curve. The first layer contains the constant degradation rates or coefficients measured during experimental testing. The second layer allows the scaling of the degradation rates with the electrochemical phenomena through scaling functions that depend on the current density. The third layer scales the degradation rates with the physical conditions of the FC stack such as the temperature and the relative humidity. The scaling functions of the second and the third layers were developed based on the effect of the electrochemical phenomena and the physical conditions on degradation mechanisms such as fluoride release rate or Pt grain size growth. This approach allows the update of the model with state-of-the-art PEMFC degradation rates measured under known operating conditions by modifying the degradation rate coefficients and calibrating the scaling functions so that their value is 1 at testing conditions. The main interest of developing this flexible model architecture lies in enabling the use of the degradation rate data generated during PEMFC degradation protocols testing, which are significantly different from the real operation, for driving cycle degradation prediction. This model was validated with experimental data from the literature of an FC city bus operating in real driving cycle conditions with an error of total degradation lower than 0.1%.

The degradation model was then applied together with an FC system model integrated into a virtual fuel cell vehicle model whose fuel cell system operates as a range-extender, i.e., FCREx architecture with a 30 kWh battery. The integrated models were simulated in WLTC 3b driving cycles with different FC stack sizing, for which the components of the balance of plant were scaled accordingly, with different dynamic limitations on the current density change rate were imposed through the energy management strategy. The results of the simulations showed how:

- Increasing the FC stack power decreased the H_2 consumption (↓ OPEX) and increased the FC stack durability at the expense of increasing the vehicle production costs (↑ CAPEX).
- Increasing the dynamic limitations increased H_2 consumption (↑ OPEX) and durability with no effect over production costs (= CAPEX). This trade-off was recommended to be considered by FCREx vehicle manufacturers.

- It was identified that at high dynamic limitations, the effect of FC stack sizing was negligible. Control strategies with dynamic limitations of 0.001 A/cm^{2}s were not recommended as they may penalize significantly H_2 consumption and prevent the vehicle from keeping the charge sustaining mode under aggressive driving conditions. Therefore, vehicle manufacturers should aim to impose dynamic limitations that provide sufficient life for the selected application and should avoid over-constrained energy management control strategies.
- The isolated effect of sizing implied a decrease in H_2 consumption of ~3% and an increase in FC stack durability of ~53% when comparing the 40 kW and 100 kW designs.
- The effect of dynamic limitations was significantly perceived in the 40 kW design which implied an increase in H_2 consumption close to 8% and an increase in durability of 294% when comparing the infinite dynamics and the highest dynamically restricted cases.

Finally, it was detected a shift in degradation rate source relevance when high dynamic limitations were applied. In this case, load-change degradation became a minor degradation source, being start–stop and low-power degradation more relevant. This might affect the design process of FC stack manufacturers for FCREx vehicles since they may be interested in prioritizing the design of low-degradation start–stop sequence or considering materials with low degradation under high-voltage conditions rather than focusing on designing the FC stack inner channels to decrease water management issues in highly-dynamic operation.

6. Research limitations, challenges, and future prospects

The main objective of this study is to develop a semi-empirical semi-physical degradation model to evaluate the change in FC stack degradation rate due to energy management strategy optimization and powertrain sizing under driving operating conditions. The idea behind this model was to make it flexible to extrapolate the degradation rates from laboratory conditions to actual driving conditions, which has been achieved as shown in Fig. 13. Nonetheless, it is imperative to understand whether the scaling functions should be tuned to directly apply the degradation rates obtained from the standardized accelerated degradation tests (proposed by the DoE or any other entity). For that purpose, it would be necessary to follow these protocols with state-of-the-art FC systems and track the progressive degradation of the stack while calibrating the degradation model. This is in the roadmap of the authors who intend to perform these tests in a 200 kW FCS testing facility.

Regarding other possible updates of the degradation model, it should be possible with the experimental data that is intended to be generated by the authors, not only estimate the change in the polarization curve of the model, but also the change in each electrochemical loss (activation, ohmic and mass transport, mainly) causing the change in the polarization curve. For that purpose, the experimental campaign proposed above should also include the monitoring of the change in the dielectric properties of the FC stack. The data obtained should help improve the amount of information that the proposed semi-empirical semi-physical degradation model can provide.

The main challenge for researchers developing degradation models for FC stacks is to develop a simulation tool capable of predicting the change in the degradation rate with the FC design and internal parameters such as the Pt loading, the membrane thickness, and the geometry of the bipolar plates. As explained in Section 1, there are some physical models accounting for these parameters (particularly the Pt loading) but their application implies a noticeable increase in the computational cost since it is required to solve additional transport equations to use them. For that reason, the final stage of the semi-empirical fast models predicting degradation is to include the effect of the FC stack inner design on durability, but for that significant amount of experimental data obtained with state-of-the-art FC stacks with different inner design accounting for degradation are required.

Finally, this study is only applied to FCREx vehicles for light-duty passenger car applications. Therefore, the use of this degradation model with other applications such as heavy-duty trucks shall bring light to the relative effect of each degradation source according to the application. In this sense, the authors have already started different studies to evaluate not only the degradation of FC stacks in heavy-duty transport applications but also the effect of alternative control strategies limitations to understand how the FC stack durability can be improved with the minimum penalty in H_2 consumption.

CRediT authorship contribution statement

J.M. Desantes: Conceptualization, Project administration, Supervision. **R. Novella:** Investigation, Formal analysis, Writing – review & editing. **B. Pla:** Resources, Methodology, Software, Data curation. **M. Lopez-Juarez:** Investigation, Methodology, Validation, Software, Writing – original draft.

Declaration of competing interest

The authors declare that they have no known competing financial interests or personal relationships that could have appeared to influence the work reported in this paper.

Acknowledgments

This research has been partially funded by the Spanish Ministry of Science, Innovation, and University through the University Faculty Training (FPU) program (FPU19/00550) and FEDER and the Generalitat Valenciana, Consellería d'Innovació, Universitats, Ciencia i Societat Digital through project IDIFEDER/2021/039.

References

[1] de Pee A, Pinner D, Roelofsen O, Somers K, Speelman E, Witteveen M. Decarbonization of industrial sectors: the next frontier. McKinsey Co 2018;(June):68.
[2] Desantes JM, Molina S, Novella R. Comparative global warming impact and NO x emissions of conventional and hydrogen automotive propulsion systems. Energy Convers Manage 2020;221(X):113137. http://dx.doi.org/10.1016/j.enconman.2020.113137.
[3] International Energy Agency. The future of hydrogen. Tech. rep, (June). 2019, http://dx.doi.org/10.1787/1e0514c4-en.
[4] Park C, Jung Y, Lim K, Kim B, Kang Y, Ju H. Analysis of a phosphoric acid fuel cell-based multi-energy hub system for heat, power, and hydrogen generation. Appl Therm Eng 2021;189(February):116715. http://dx.doi.org/10.1016/j.applthermaleng.2021.116715.
[5] He Y, Zhou Y, Yuan J, Liu Z, Wang Z, Zhang G. Transformation towards a carbon-neutral residential community with hydrogen economy and advanced energy management strategies. Energy Convers Manage 2021;249(October):114834. http://dx.doi.org/10.1016/j.enconman.2021.114834.
[6] Liu J, Yang H, Zhou Y. Peer-to-peer trading optimizations on net-zero energy communities with energy storage of hydrogen and battery vehicles. Appl Energy 2021;302(August):117578. http://dx.doi.org/10.1016/j.apenergy.2021.117578.
[7] Liu J, Yang H, Zhou Y. Peer-to-peer energy trading of net-zero energy communities with renewable energy systems integrating hydrogen vehicle storage. Appl Energy 2021;298(February):117206. http://dx.doi.org/10.1016/j.apenergy.2021.117206.
[8] He Y, Zhou Y, Wang Z, Liu J, Liu Z, Zhang G. Quantification on fuel cell degradation and techno-economic analysis of a hydrogen-based grid-interactive residential energy sharing network with fuel-cell-powered vehicles. Appl Energy 2021;303(August):117444. http://dx.doi.org/10.1016/j.apenergy.2021.117444.
[9] Feroldi D, Carignano M. Sizing for fuel cell/supercapacitor hybrid vehicles based on stochastic driving cycles. Appl Energy 2016;183:645–58. http://dx.doi.org/10.1016/j.apenergy.2016.09.008.
[10] Molina S, Novella R, Pla B, Lopez-Juarez M. Optimization and sizing of a fuel cell range extender vehicle for passenger car applications in driving cycle conditions. Appl Energy 2021;285(December 2020):116469. http://dx.doi.org/10.1016/j.apenergy.2021.116469.

[11] Desantes J, Novella R, Pla B, Lopez-Juarez M. Impact of fuel cell range extender powertrain design on greenhouse gases and NOX emissions in automotive applications. Appl Energy 2021;302:117526. http://dx.doi.org/10.1016/j.apenergy.2021.117526.

[12] Xu L, Ouyang M, Li J, Yang F, Lu L, Hua J. Optimal sizing of plug-in fuel cell electric vehicles using models of vehicle performance and system cost. Appl Energy 2013;103(2013):477–87. http://dx.doi.org/10.1016/j.apenergy.2012.10.010.

[13] Wu Z, Wang C, Wolfram P, Zhang Y, Sun X, Hertwich E. Assessing electric vehicle policy with region-specific carbon footprints. Appl Energy 2019;256(7491):113923. http://dx.doi.org/10.1016/j.apenergy.2019.113923.

[14] Wu X, Hu X, Yin X, Peng Y, Pickert V. Convex programming improved online power management in a range extended fuel cell electric truck. J Power Sources 2020;476(2019):228642. http://dx.doi.org/10.1016/j.jpowsour.2020.228642.

[15] McKinsey. A portfolio of power-trains for Europe: a fact-based analysis - The role of battery electric vehicles, plug-in hybrids and fuel cell electric vehicles. Tech. rep, 2020, p. 68.

[16] Office of energy efficiency and renewable energy - Department of Energy. Durability Working Group - Hydrogen and Fuel Cell Technologies Office.

[17] Qin Y, Liu G, Chang Y, Du Q. Modeling and design of PEM fuel cell stack based on a flow network method. Appl Therm Eng 2018;144(August):411–23. http://dx.doi.org/10.1016/j.applthermaleng.2018.08.050.

[18] Pan T, Shen J, Sun L, Lee KY. Thermodynamic modelling and intelligent control of fuel cell anode purge. Appl Therm Eng 2019;154(March):196–207. http://dx.doi.org/10.1016/j.applthermaleng.2019.03.009.

[19] Li H, Ravey A, N'Diaye A, Djerdir A. Online adaptive equivalent consumption minimization strategy for fuel cell hybrid electric vehicle considering power sources degradation. Energy Convers Manage 2019;192(March):133–49. http://dx.doi.org/10.1016/j.enconman.2019.03.090.

[20] Chen B, Cai Y, Shen J, Tu Z, Chan SH. Performance degradation of a proton exchange membrane fuel cell with dead-ended cathode and anode. Appl Therm Eng 2018;132:80–6. http://dx.doi.org/10.1016/j.applthermaleng.2017.12.078.

[21] Cherevko S, Kulyk N, Mayrhofer KJ. Durability of platinum-based fuel cell electrocatalysts: Dissolution of bulk and nanoscale platinum. Nano Energy 2016;29:275–98. http://dx.doi.org/10.1016/j.nanoen.2016.03.005.

[22] Zheng W, Xu L, Hu Z, Ding Y, Li J, Ouyang M. Dynamic modeling of chemical membrane degradation in polymer electrolyte fuel cells: Effect of pinhole formation. J Power Sources 2021;487(December 2020):229367. http://dx.doi.org/10.1016/j.jpowsour.2020.229367.

[23] Moein-Jahromi M, Kermani MJ. Three-dimensional multiphase simulation and multi-objective optimization of PEM fuel cells degradation under automotive cyclic loads. Energy Convers Manage 2021;231(February):113837. http://dx.doi.org/10.1016/j.enconman.2021.113837.

[24] Terada I, Nakagawa H. Polymer electrolyte fuel cell. Kobunshi 2008;57(7):498–501. http://dx.doi.org/10.1295/kobunshi.57.498.

[25] Shi S, Sun X, Lin Q, Chen J, Fu Y, Hong X, et al. Fatigue crack propagation behavior of fuel cell membranes after chemical degradation. Int J Hydrogen Energy 2020;45(51):27653–64. http://dx.doi.org/10.1016/j.ijhydene.2020.07.113.

[26] Yuan XZ, Nayoze-Coynel C, Shaigan N, Fisher D, Zhao N, Zamel N, et al. A review of functions, attributes, properties and measurements for the quality control of proton exchange membrane fuel cell components. J Power Sources 2021;491(January):229540. http://dx.doi.org/10.1016/j.jpowsour.2021.229540.

[27] Chen H, Song Z, Zhao X, Zhang T, Pei P, Liang C. A review of durability test protocols of the proton exchange membrane fuel cells for vehicle. Appl Energy 2018;224(April):289–99. http://dx.doi.org/10.1016/j.apenergy.2018.04.050.

[28] Pei P, Chang Q, Tang T. A quick evaluating method for automotive fuel cell lifetime. Int J Hydrogen Energy 2008;33(14):3829–36. http://dx.doi.org/10.1016/j.ijhydene.2008.04.048.

[29] Lu L, Ouyang M, Huang H, Pei P, Yang F. A semi-empirical voltage degradation model for a low-pressure proton exchange membrane fuel cell stack under bus city driving cycles. J Power Sources 2007;164(1):306–14. http://dx.doi.org/10.1016/j.jpowsour.2006.10.061.

[30] Song K, Wang X, Li F, Sorrentino M, Zheng B. Pontryagin's minimum principle-based real-time energy management strategy for fuel cell hybrid electric vehicle considering both fuel economy and power source durability. Energy 2020;205:118064. http://dx.doi.org/10.1016/j.energy.2020.118064.

[31] Peng F, Zhao Y, Chen T, Zhang X, Chen W, Zhou D, et al. Development of robust suboptimal real-time power sharing strategy for modern fuel cell based hybrid tramways considering operational uncertainties and performance degradation. Appl Energy 2018;226(April):503–21. http://dx.doi.org/10.1016/j.apenergy.2018.05.092.

[32] Sun Z, Wang Y, Chen Z, Li X. Min-max game based energy management strategy for fuel cell/supercapacitor hybrid electric vehicles. Appl Energy 2020;267(January):115086. http://dx.doi.org/10.1016/j.apenergy.2020.115086.

[33] Hu Z, Li J, Xu L, Song Z, Fang C, Ouyang M, et al. Multi-objective energy management optimization and parameter sizing for proton exchange membrane hybrid fuel cell vehicles. Energy Convers Manage 2016;129:108–21. http://dx.doi.org/10.1016/j.enconman.2016.09.082.

[34] Zhou Y, Obeid H, Laghrouche S, Hilairet M, Djerdir A. A novel second-order sliding mode control of hybrid fuel cell/super capacitors power system considering the degradation of the fuel cell. Energy Convers Manage 2021;229(September 2020):113766. http://dx.doi.org/10.1016/j.enconman.2020.113766.

[35] Ou M, Zhang R, Shao Z, Li B, Yang D, Ming P, et al. A novel approach based on semi-empirical model for degradation prediction of fuel cells. J Power Sources 2021;488(December 2020):229435. http://dx.doi.org/10.1016/j.jpowsour.2020.229435.

[36] Ma R, Yang T, Breaz E, Li Z, Briois P, Gao F. Data-driven proton exchange membrane fuel cell degradation predication through deep learning method. Appl Energy 2018;231(July):102–15. http://dx.doi.org/10.1016/j.apenergy.2018.09.111.

[37] Chen K, Laghrouche S, Djerdir A. Degradation model of proton exchange membrane fuel cell based on a novel hybrid method. Appl Energy 2019;252(May):113439. http://dx.doi.org/10.1016/j.apenergy.2019.113439.

[38] Bressel M, Hilairet M, Hissel D, Ould Bouamama B. Extended Kalman filter for prognostic of proton exchange membrane fuel cell. Appl Energy 2016;164:220–7. http://dx.doi.org/10.1016/j.apenergy.2015.11.071.

[39] Jha MS, Bressel M, Ould-Bouamama B, Dauphin-Tanguy G. Particle filter based hybrid prognostics of proton exchange membrane fuel cell in bond graph framework. Comput Chem Eng 2016;95:216–30. http://dx.doi.org/10.1016/j.compchemeng.2016.08.018.

[40] Kregar A, Tavčar G, Kravos A, Katrašnik T. Predictive system-level modeling framework for transient operation and cathode platinum degradation of high temperature proton exchange membrane fuel cells . Appl Energy 2020;263(February):114547. http://dx.doi.org/10.1016/j.apenergy.2020.114547.

[41] Li Y, Chen X, Liu Y, Xiong D, Li J, et al. Analytical modeling framework for performance degradation of PEM fuel cells during startup-shutdown cycles. RSC Adv 2020;10(4):2216–26. http://dx.doi.org/10.1039/c9ra09572a.

[42] Kwon JH, Jo S, Cho KY, Eom KS. Deconvolution of the dehydration degradation mechanism in polymer electrolyte membrane fuel cells using electrochemical impedance analysis combined with the transmission line model under low humidity. J Power Sources 2020;473(March):228587. http://dx.doi.org/10.1016/j.jpowsour.2020.228587.

[43] Futter GA, Latz A, Jahnke T. Physical modeling of chemical membrane degradation in polymer electrolyte membrane fuel cells: Influence of pressure, relative humidity and cell voltage. J Power Sources 2019;410–411(November 2018):78–90. http://dx.doi.org/10.1016/j.jpowsour.2018.10.085.

[44] Teng T, Zhang X, Dong H, Xue Q. A comprehensive review of energy management optimization strategies for fuel cell passenger vehicle. Int J Hydrogen Energy 2020;(xxxx). http://dx.doi.org/10.1016/j.ijhydene.2019.12.202.

[45] Ballard. Product data sheet - FCVelocity-MD. 2016.

[46] Ballard. Product data sheet - FCMove-HD. 2016.

[47] Murschenhofer D, Kuzdas D, Braun S, Jakubek S. A real-time capable quasi-2D proton exchange membrane fuel cell model. Energy Convers Manage 2018;162(January):159–75. http://dx.doi.org/10.1016/j.enconman.2018.02.028.

[48] Corbo P, Migliardini F, Veneri O. Experimental analysis and management issues of a hydrogen fuel cell system for stationary and mobile application. Energy Convers Manage 2007;48(8):2365–74. http://dx.doi.org/10.1016/j.enconman.2007.03.009.

[49] Corbo P, Migliardini F, Veneri O. Experimental analysis of a 20 kWe PEM fuel cell system in dynamic conditions representative of automotive applications. Energy Convers Manage 2008;49(10):2688–97. http://dx.doi.org/10.1016/j.enconman.2008.04.001.

[50] Onori S, Serrao L, Rizzoni G. Hybrid electric vehicles: energy management strategies. Springer; 2016.

[51] Luján JM, Guardiola C, Pla B, Reig A. Cost of ownership-efficient hybrid electric vehicle powertrain sizing for multi-scenario driving cycles. Proc Inst Mech Eng D 2016;230(3):382–94.

[52] Serrao L, Onori S, Rizzoni G. ECMS as a realization of pontryagin's minimum principle for HEV control. In: 2009 american control conference. IEEE; 2009, p. 3964–9.

[53] Tsotridis G, Pilenga A, Marco GD, Malkow T. EU Harmonised test protocols for PEMFC MEA testing in single cell configuration for automotive applications: JRC science for policy report. Tech. rep, European Commission, JRC Science for Policy report; 2015, p. 60. http://dx.doi.org/10.2790/54653.

[54] Garland N, Benjamin T, Kopasz J. DOE Fuel cell program: Durability technical targets and testing protocols. ECS - Electrochem Soc ECS Trans 2007;11(1):923. http://dx.doi.org/10.1149/1.2781004.

[55] DoE - Department of Energy. DOE Technical Targets for Polymer Electrolyte Membrane Fuel Cell Components.

[56] Song K, Chen H, Wen P, Zhang T, Zhang B, Zhang T. A comprehensive evaluation framework to evaluate energy management strategies of fuel cell electric vehicles. Electrochim Acta 2018;292:960–73. http://dx.doi.org/10.1016/j.electacta.2018.09.166.

[57] Marocco P, Sundseth K, Aarhaug T, Lanzini A, Santarelli M, Barnett AO, et al. Online measurements of fluoride ions in proton exchange membrane water electrolysis through ion chromatography. J Power Sources 2021;483(October 2020):229179. http://dx.doi.org/10.1016/j.jpowsour.2020.229179.

[58] Kusoglu A, Calabrese M, Weber AZ. Effect of mechanical compression on chemical degradation of Nafion membranes. ECS Electrochem Lett 2014;3(5). http://dx.doi.org/10.1149/2.008405eel.

[59] Bhosale AC, Meenakshi S, Ghosh PC. Root cause analysis of the degradation in a unitized regenerative fuel cell. J Power Sources 2017;343:275–83. http://dx.doi.org/10.1016/j.jpowsour.2017.01.060.

[60] Hu Z, Xu L, Huang Y, Li J, Ouyang M, Du X, et al. Comprehensive analysis of galvanostatic charge method for fuel cell degradation diagnosis. Appl Energy 2018;212(October 2017):1321–32. http://dx.doi.org/10.1016/j.apenergy.2018.01.005.

[61] Knights S. Polymer electrolyte membrane and direct methanol fuel cell technology: 6 - operation and durability of low temperature fuel cells, Vol. 1. Woodhead Publishing Limited; 2012, p. 137–77. http://dx.doi.org/10.1533/9780857095473.2.137.

[62] Kangasniemi KH, Condit DA, Jarvi TD. Characterization of Vulcan electrochemically oxidized under simulated PEM fuel cell conditions. J Electrochem Soc 2004;151(4):E125. http://dx.doi.org/10.1149/1.1649756.

[63] Feng Y, Dong Z. Integrated design and control optimization of fuel cell hybrid mining truck with minimized lifecycle cost. Appl Energy 2020;270(March):115164. http://dx.doi.org/10.1016/j.apenergy.2020.115164.

[64] Zhao J, Li X. A review of polymer electrolyte membrane fuel cell durability for vehicular applications: Degradation modes and experimental techniques. Energy Convers Manage 2019;199(September 2019):112022. http://dx.doi.org/10.1016/j.enconman.2019.112022.

[65] Zawodzinski TA, Springer TE, Davey J, Jestel R, Lopez C, Valerio J, et al. A comparative study of water uptake by and transport through ionomeric fuel cell membranes. J Electrochem Soc 1993;140(7):1981–5. http://dx.doi.org/10.1149/1.2220749.

[66] Barbir F. PEM fuel cells theory and practice chapter 4 - main cell components, material properties, and processes. In: PEM fuel cells. 2013, p. 73–117. http://dx.doi.org/10.1016/b978-0-12-387710-9.00004-7.

[67] Bi W, Fuller TF. Temperature effects on PEM fuel cells PtC catalyst degradation. J Electrochem Soc 2008;155(2):B215. http://dx.doi.org/10.1149/1.2819680.

[68] Jia N, Dutta M, Lu S, Colbow V. Voltage degradation associated with operational conditions: Upper potential and lower potential limits. J Electrochem Soc 2009;2–3. http://dx.doi.org/10.1149/ma2009-02/10/960.

[69] Borup RL, Davey J, Wood D, Garzon F, Inbody M. DOE hydrogen program FY 2005 progress report - VII.I.3 PEM fuel cell durability. Tech. rep., 2005, p. 1039–45.

[70] Mathias MF, Makharia R, Gasteiger HA, Conley JJ, Fuller TJ, Gittleman CJ, et al. Two fuel cell cars in every garage? Electrochem Soc Interface 2005;14(3):24–35.

[71] Dutta M, Jia N, Lu S, Colbow V, Wessel S. Effects of upper potential dwell time, transients and relative humidity on PEM fuel cell cathode catalyst degradation. In: The electrochemical society 217th meeting (c). 2010.

[72] Wu J, Yuan XZ, Martin JJ, Wang H, Zhang J, Shen J, et al. A review of PEM fuel cell durability: Degradation mechanisms and mitigation strategies. J Power Sources 2008;184(1):104–19. http://dx.doi.org/10.1016/j.jpowsour.2008.06.006.

[73] Bezmalinovic D, Simic B, Barbir F. Characterization of PEM fuel cell degradation by polarization change curves. J Power Sources 2015;294:82–7. http://dx.doi.org/10.1016/j.jpowsour.2015.06.047.